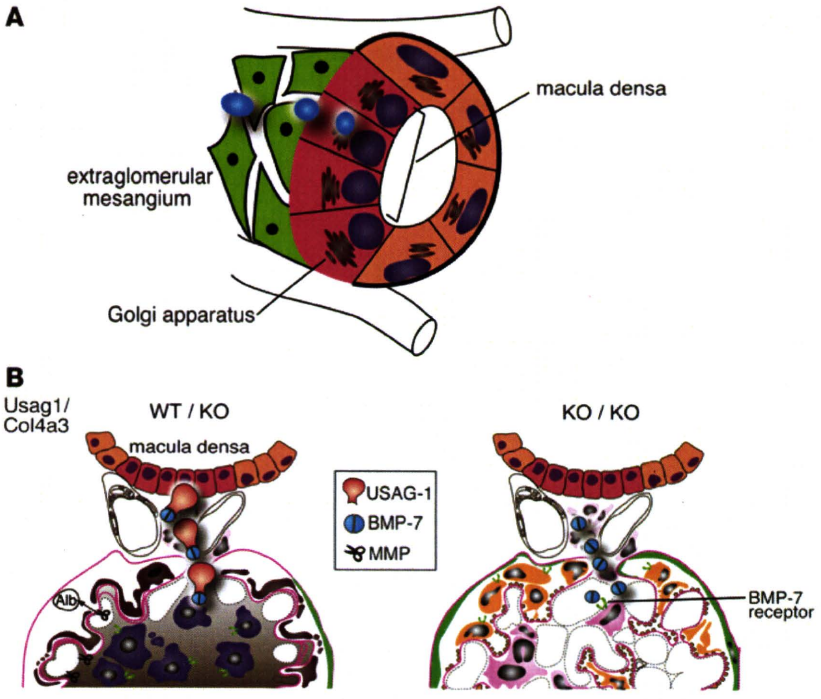

Figure 7
Hypothetical model for involvement of USAG-1 secreted from distal tubules in the pathogenesis of glomerular damage in Alport syndrome. (**A**) The macula densa (red), a part of the distal tubules, lies beside the extraglomerular mesangial cells (green), and the nuclei of the macula densa cells are apically located, suggesting the possibility that substances (blue) might be secreted from the basolateral membrane of the macula densa. Note that the basement membrane of the macula densa cells is continuous with the basement membrane of the extraglomerular mesangial cells. (**B**) In *Usag1*$^{+/+}$*Col4a3*$^{-/-}$ mice (WT/KO), the mesangial cells are activated (purple) and secrete MMPs (scissors), which degrade GBM. Following GBM destruction, podocytes residing on the GBM are damaged (brown) and albuminuria is observed. BMP-7 (blue) secreted from the macula densa is captured by USAG-1, which is also secreted from the macula densa. As a consequence, BMP-7 cannot bind to its receptors and exert its renoprotective action. In *Usag1*$^{-/-}$*Col4a3*$^{-/-}$ mice (KO/KO), BMP-7 secreted from the macula densa can bind to its receptors on mesangial cells and podocytes, and protect fragile alport GBM from degradation.

lus. The signals from the macula densa to the mesangial cells involve small diffusible substances (ATP or adenosine) released from the macula densa (47, 54). Multiphoton imaging demonstrates the water flow across the macula densa into the mesangial cell field at varying osmolarities in the luminal fluid (47). The histological characteristics of the macula densa also support the idea of substance transportation from the macula densa to mesangial cells: the nuclei of macula densa cells are apically located, while most of cell organelles tend to be located basally and laterally, thus indicating that the substances from the macula densa are possibly secreted basolaterally (Figure 7A). In addition, the basement membrane of the macula densa is fused with the basement membrane of the extraglomerular mesangial cells, indicating the lack of a barrier to interfere with the substance transportation from the macula densa to the glomerulus (Figure 7A). Furthermore, Hugo et al. demonstrated that extraglomerular mesangial cells function as reserve cells for glomerular mesangial cells (55). Extraglomerular mesangial cells stimulated by substances secreted from the macula densa migrate into glomerulus after glomerular injury and repopulate as mesangial cells.

As shown in Figure 6C, both USAG-1 and BMP-7 are expressed in the macula densa, and USAG-1 secreted from the basolateral membrane of macula densa could inhibit the action of BMP-7 on the adjacent mesangial cells. In the experiments using cultured mesangial cells, BMP-7 significantly attenuated TGF-β–induced MMP-12 upregulation, and the inhibitory effect of BMP-7 was abolished by the addition of USAG-1. Moreover, BMP-7 reduced TGF-β–induced cytotoxicity in mesangial cells (data not shown). Therefore, USAG-1 might exacerbate glomerular pathogenesis in Alport syndrome through accelerating upregulation of GBM-degrading enzyme and cytotoxicity by inhibiting the reno-protective effects of BMP-7 (Figure 7B).

An alternative possibility that may explain the effect of USAG-1 on glomerular injury is an interaction between circulating USAG-1 and BMP-7 in plasma. BMP-7 is present in plasma at a concentration range of 100–300 pg/ml (12). Due to the lack of an effective ELISA system, the plasma level of USAG-1 remains to be determined. If an appropriate amount of USAG-1 is present in the circulation, it could therefore bind to BMP-7 and thus inhibit its activity. To test the effect of circulating USAG-1 in the progression of *Col4a3*$^{-/-}$ mice, we performed systemic gene transfer of USAG-1 expression vector to *Usag1*$^{-/-}$*Col4a3*$^{-/-}$ mice and demonstrated that the difference in albuminuria between the gene transfer group and the control group was not statistically significant (Supplemental Figure 3).

Novel therapeutic approach for Alport syndrome. At present there is no definitive therapy to prevent or slow renal disease progression in Alport syndrome. Several studies using a mouse model of Alport syndrome have provided potential therapies, such as MMP inhibitor (29, 40), angiotensin-converting enzyme inhibitor (56), statins (57), transplantation of bone marrow–derived stem cells (58–60), and total body irradiation (61). The results of the present study support the notion that therapeutic trials to inhibit the function of USAG-1 may become a novel therapeutic approach for Alport syndrome either alone or in combination with other approaches. A therapeutic trial targeting USAG-1 is promising because it is expected to be effective in both glomerular and tubular injuries, is more kidney-specific, and has fewer extrarenal effects because the expression of USAG-1 is confined to the kidney.

Methods

Mice. The *Usag1*$^{-/-}$ mice used in this study have been described previously (27), and *Col4a3*$^{-/-}$ mice were purchased from Jackson Laboratory (JAX mice strain 129-Col4a3^{tm1Dec}/J) (62). *Usag1*$^{-/-}$*Col4a3*$^{-/-}$ mice were generated by breeding *Usag1*$^{+/-}$ and *Col4a3*$^{+/-}$ mice. *Col4a3*$^{-/-}$ littermates (*Usag1*$^{+/+}$*Col4a3*$^{-/-}$ mice) and WT littermates (*Usag1*$^{+/+}$*Col4a3*$^{+/+}$ mice) served as controls. All animal studies were approved by the Animal Research Committee, Graduate School of Medicine, Kyoto University, and performed in accordance with the guidelines of Kyoto University.

Age-matched mice were used for all studies. The ages of mice used in each experiment are described below.

Assessment of albuminuria. The mice were placed in metabolic cages, and urine was collected over a 24-hour period. During the urine collection, mice were allowed free access to food and water. Urinary albumin concentration was measured using the Albuwell M assay kit (Exocell).

Renal histopathology and electron microscopy. The kidneys were fixed in Carnoy's solution and embedded in paraffin. Sections (2-μm thick) were stained with PAS for routine histological examination, and the degree of morphological change was determined for ten 10-week-old mice and five 6-week-old mice per group by experienced pathologists who were blinded to the genotypes. The following parameters were evaluated: percentage of hemorrhagic glomeruli and sclerotic glomeruli; and tubular atrophy/interstitial fibrosis score. Tubular atrophy/interstitial fibrosis was graded as follows: grade 0, 0%–24%; grade 1, 25%–49%; grade 2, 50%–74%; grade 3, ≥ 75%.

Frozen sections of the kidneys were immunostained as previously described (63). The primary antibodies were against podocin (64), α1 (H11), and α3 (H31) chains of type IV collagen (a gift from Y. Sado; ref. 65), MCP-1 (R&D Systems), MMP-12 (Santa Cruz Biotechnology Inc.), nNOS (Cayman Chemical and Abcam), and LacZ (Cappel Laboratory). For double staining with β-gal, immunostaining was performed before β-gal staining to avoid the possibility that the deposition of X-gal might interfere with the antibody binding to the antigen. For electron microscopy, portions of the cortex were fixed in 2% glutaraldehyde and post-fixed in 1% osmic acid. After embedding, ultrathin sections were stained with uranyl acetate and lead citrate.

β-Gal staining and in situ hybridization. β-Gal staining and in situ hybridization were performed as described previously (26, 66). The probe for in situ hybridization of *USAG-1* mRNA contained the 1.0-kb open reading frame with GC content of 52.6%. Hybridization was detected using an anti-digoxigenin antibody conjugated with alkaline phosphatase and Nitro blue tetrazolium chloride/5-bromo-4-chloro-3-indolyl phosphate, 4-toluidine salt (Roche Diagnostics).

Immunoblotting. Whole-kidney tissue was homogenized in RIPA buffer and subjected to immunoblotting as previously described (67). The primary antibodies were anti-phospho-Smad1/5/8 (Cell Signaling Technology), phospho-Smad2 (Upstate Biotechnology), and GAPDH (Fitzgerald Industries).

Quantification of mRNA by real-time RT-PCR. Real-time RT-PCR was performed as described previously (27). Specific primers were designed using Primer Express software (Applied Biosystems). Serially diluted cDNA was used to generate the standard curve for each primer, and the PCR conditions were as follows: 50°C for 2 minutes, 95°C for 10 minutes, then 95°C for 15 seconds, and 60°C for 1 minute for 40 cycles.

Cell cultures. Mouse mesangial cells were established from glomeruli isolated from a 4-week-old normal mouse (C57BL/6J) and characterized as described previously (68). Cells of passage numbers 18 to 21 were cultured in DMEM/F12 containing 20% fetal calf serum.

Assessment of MMP mRNA expression in mesangial cells. Mesangial cells were seeded at a concentration of 5×10^4/ml. After 24 hours, the culture medium was replaced with DMEM containing 0.5% bovine serum albumin. The cells were incubated for 72 hours with 10 ng/ml MCP-1 (R&D Systems), 250 pg/ml IL-1β (R&D Systems), or 3 ng/ml TGF-β (R&D Systems) in the presence or absence of 20 ng/ml BMP-7 (R&D Systems) and then were analyzed for *MMP* mRNA expression by real-time RT-PCR. All experiments were performed in quadruplicate.

Production of recombinant USAG-1–Flag protein. A recombinant C-terminally Flag-tagged USAG-1 protein (USAG-1–Flag) was produced using the Baculovirus Expression System (Invitrogen) and purified from culture medium by affinity absorption on anti-FLAG M2 affinity beads (Sigma-Aldrich). Protein concentrations were estimated by Coomassie staining.

Zymography. Renal proteins were extracted as previously described (69). Samples standardized for protein concentration of 60 μg/lane were electrophoretically separated in 10% SDS-polyacrylamide gels that contained 1 mg/ml gelatin or α-casein. After separation, gels were placed in 2.5% Triton X-100 in PBS, washed, and incubated in developing buffer (50 mM Tris, pH 7.5, 200 mM NaCl, 5 mM CaCl2, and 0.02% Brij-35) overnight at 37°C. The gels were stained with 0.5% Coomassie blue R250 and then destained with a 10% acetic acid, 40% methanol solution until the gelatinolytic bands were clearly seen.

Systemic gene transfer. *Usag1*$^{-/-}$*Col4a3*$^{-/-}$ mice were injected with 300 μg of pcDNA3.1mUSAG-1 (cDNA for mouse USAG-1 cloned into the pcDNA3.1 expression vector) into the tibialis anterior muscle at 6 weeks as described (70) and were analyzed at 8 weeks for urinary albumin and renal histology.

Statistics. Data are presented as the mean ± SD. Statistical significance was assessed by Student's *t* test for 2 group comparisons and by ANOVA, followed by Fisher's protected least significant difference post-hoc test for multiple group comparisons. Significance was defined as a value of $P < 0.05$.

Acknowledgments

We thank Y. Kaziro, Y. Nabeshima, and T. Nakamura for valuable comments and discussion. We also thank Y. Sado for excellent subtype-specific antibodies against type IV collagen and J. Nakamura, N. Suzuki, and A. Hosotani for excellent technical assistance. This study was supported by grants-in-aid from the Ministry of Education, Culture, Science, Sports, and Technology of Japan (Wakate 177090551; Ho-ga 19659219; Kiban C 20590954), a grant-in-aid for Research on Biological Markers for New Drug Development, Health and Labour Sciences research grants from the Ministry of Health, Labor, and Welfare of Japan (08062855), a grant from the Astellas Foundation for Research on Metabolic Disorders, a grant from the Novartis Foundation for the promotion of science, a grant from the Kato Memorial Trust for Nambyo Research, a grant from the Hayashi Memorial Foundation for Female Natural Scientists, a grant from the Takeda Science Foundation, and a grant from the Japan Foundation for Applied Enzymology.

Received for publication November 24, 2009, and accepted December 16, 2009.

Address correspondence to: Motoko Yanagita, Career-Path Promotion Unit for Young Life Scientists, Kyoto University Graduate School of Medicine, Yoshida-konoe-cho, Sakyo-ku, Kyoto 606-8501, Japan. Phone: 81.75.753.9310; Fax: 81.75.753.9311; E-mail: motoy@kuhp.kyoto-u.ac.jp.

1. Kalluri R. Basement membranes: structure, assembly and role in tumour angiogenesis. *Nat Rev Cancer.* 2003;3(6):422–433.
2. Timpl R. Structure and biological activity of basement membrane proteins. *Eur J Biochem.* 1989;180(3):487–502.
3. Hudson BG, Tryggvason K, Sundaramoorthy M, Neilson EG. Alport's syndrome, Goodpasture's syndrome, and type IV collagen. *N Engl J Med.* 2003; 348(25):2543–2556.
4. Pescucci C, Longo I, Bruttini M, Mari F, Renieri A. Type-IV collagen related diseases. *J Nephrol.* 2003;16(2):314–316.
5. Barker DF, et al. Identification of mutations in the COL4A5 collagen gene in Alport syndrome. *Science.* 1990;248(4960):1224–1227.
6. Lemmink HH, et al. Mutations in the type IV collagen alpha 3 (COL4A3) gene in autosomal recessive Alport syndrome. *Hum Mol Genet.* 1994;3(8):1269–1273.
7. Mochizuki T, et al. Identification of mutations in the alpha 3(IV) and alpha 4(IV) collagen genes in autosomal recessive Alport syndrome. *Nat Genet.* 1994;8(1):77–81.
8. Zoja C, Morigi M, Benigni A, Remuzzi G. Genetics of rare diseases of the kidney: learning from mouse models. *Cytogenet Genome Res.* 2004;

105(2–4):479–484.
9. Kalluri R, Shield CF, Todd P, Hudson BG, Neilson EG. Isoform switching of type IV collagen is developmentally arrested in X-linked Alport syndrome leading to increased susceptibility of renal basement membranes to endoproteolysis. *J Clin Invest.* 1997;99(10):2470–2478.
10. Massague J, Chen YG. Controlling TGF-beta signaling. *Genes Dev.* 2000;14(6):627–644.
11. Helder MN, et al. Expression pattern of osteogenic protein-1 (bone morphogenetic protein-7) in human and mouse development. *J Histochem Cytochem.* 1995;43(10):1035–1044.
12. Vukicevic S, et al. Osteogenic protein-1 (bone morphogenetic protein-7) reduces severity of injury after ischemic acute renal failure in rat. *J Clin Invest.* 1998;102(1):202–214.
13. Zeisberg M, et al. Bone morphogenic protein-7 inhibits progression of chronic renal fibrosis associated with two genetic mouse models. *Am J Physiol Renal Physiol.* 2003;285(6):F1060–F1067.
14. Zeisberg M, et al. BMP-7 counteracts TGF-beta1-induced epithelial-to-mesenchymal transition and reverses chronic renal injury. *Nat Med.* 2003;9(7):964–968.
15. Morrissey J, Hruska K, Guo G, Wang S, Chen Q, Klahr S. Bone morphogenetic protein-7 improves renal fibrosis and accelerates the return of renal function. *J Am Soc Nephrol.* 2002;13(Suppl 1):S14–S21.
16. Hruska KA. Treatment of chronic tubulointerstitial disease: a new concept. *Kidney Int.* 2002; 61(5):1911–1922.
17. Hruska KA, Guo G, Wozniak M, Martin D, Miller S, Liapis H, Loveday K, Klahr S, Sampath TK, Morrissey J. Osteogenic protein-1 prevents renal fibrogenesis associated with ureteral obstruction. *Am J Physiol Renal Physiol.* 2000;279(1):F130–F143.
18. Hruska KA, Saab G, Chaudhary LR, Quinn CO, Lund RJ, Surendran K. Kidney-bone, bone-kidney, and cell-cell communications in renal osteodystrophy. *Semin Nephrol.* 2004;24(1):25–38.
19. Zeisberg M, Shah AA, Kalluri R. Bone morphogenic protein-7 induces mesenchymal to epithelial transition in adult renal fibroblasts and facilitates regeneration of injured kidney. *J Biol Chem.* 2005;280(9):8094–8100.
20. Wang S, de Caestecker M, Kopp J, Mitu G, Lapage J, Hirschberg R. Renal bone morphogenetic protein-7 protects against diabetic nephropathy. *J Am Soc Nephrol.* 2006;17(9):2504–2512.
21. Reddi AH. Interplay between bone morphogenetic proteins and cognate binding proteins in bone and cartilage development: noggin, chordin and DAN. *Arthritis Res.* 2001;3(1):1–5.
22. Yanagita M. BMP antagonists: Their roles in development and involvement in pathophysiology. *Cytokine Growth Factor Rev.* 2005;16(3):309–317.
23. Yanagita M. Modulator of bone morphogenetic protein activity in the progression of kidney diseases. *Kidney Int.* 2006; 70(6):989–993.
24. Eddy AA. Ramping up endogenous defences against chronic kidney disease. *Nephrol Dial Transplant.* 2006;21(5):1174–1177.
25. Yanagita M, et al. USAG-1: a bone morphogenetic protein antagonist abundantly expressed in the kidney. *Biochem Biophys Res Commun.* 2004; 316(2):490–500.
26. Tanaka M, et al. Expression of BMP-7 and USAG-1 (a BMP antagonist) in kidney development and injury. *Kidney Int.* 2008;73(2):181–191.
27. Yanagita M, et al. Uterine sensitization-associated gene-1 (USAG-1), a novel BMP antagonist expressed in the kidney, accelerates tubular injury. *J Clin Invest.* 2006;116(1):70–79.
28. Sayers R, Kalluri R, Rodgers KD, Shield CF, Meehan DT, Cosgrove D. Role for transforming growth factor-beta1 in alport renal disease progression. *Kidney Int.* 1999;56(5):1662–1673.
29. Rao VH, et al. Role for macrophage metalloelastase in glomerular basement membrane damage associated with alport syndrome. *Am J Pathol.* 2006;169(1):32–46.
30. Schmierer B, Hill CS. TGFbeta-SMAD signal transduction: molecular specificity and functional flexibility. *Nat Rev Mol Cell Biol.* 2007;8(12):970–982.
31. Wang SN, Lapage J, Hirschberg R. Loss of tubular bone morphogenetic protein-7 in diabetic nephropathy. *J Am Soc Nephrol.* 2001;12(11):2392–2399.
32. Daly AC, Randall RA, Hill CS. Transforming growth factor beta-induced Smad1/5 phosphorylation in epithelial cells is mediated by novel receptor complexes and is essential for anchorage-independent growth. *Mol Cell Biol.* 2008;28(22):6889–6902.
33. Goumans MJ, et al. Activin receptor-like kinase (ALK)1 is an antagonistic mediator of lateral TGFbeta/ALK5 signaling. *Mol Cell.* 2003;12(4):817–828.
34. Pannu J, Nakerakanti S, Smith E, ten Dijke P, Trojanowska M. Transforming growth factor-beta receptor type I-dependent fibrogenic gene program is mediated via activation of Smad1 and ERK1/2 pathways. *J Biol Chem.* 2007;282(14):10405–10413.
35. Kim JH, Ryu KH, Jung KW, Han CK, Kwak WJ, Cho YB. SKI306X suppresses cartilage destruction and inhibits the production of matrix metalloproteinase in rabbit joint cartilage explant culture. *J Pharmacol Sci.* 2005;98(3):298–306.
36. Kaneko Y, et al. Macrophage metalloelastase as a major factor for glomerular injury in anti-glomerular basement membrane nephritis. *J Immunol.* 2003;170(6):3377–3385.
37. Vos CM, van Haastert ES, de Groot CJ, van der Valk P, de Vries HE. Matrix metalloproteinase-12 is expressed in phagocytotic macrophages in active multiple sclerosis lesions. *J Neuroimmunol.* 2003;138(1–2):106–114.
38. Eddy AA. Molecular insights into renal interstitial fibrosis. *J Am Soc Nephrol.* 1996;7(12):2495–2508.
39. van Kooten C, Daha MR, van Es LA. Tubular epithelial cells: A critical cell type in the regulation of renal inflammatory processes. *Exp Nephrol.* 1999;7(5–6):429–437.
40. Zeisberg M, et al. Stage-specific action of matrix metalloproteinases influences progressive hereditary kidney disease. *PLoS Med.* 2006;3(4):e100.
41. Mitu GM, Wang S, Hirschberg R. BMP7 is a podocyte survival factor and rescues podocytes from diabetic injury. *Am J Physiol Renal Physiol.* 2007;293(5):F1641–F1648.
42. De Petris L, Hruska KA, Chiechio S, Liapis H. Bone morphogenetic protein-7 delays podocyte injury due to high glucose. *Nephrol Dial Transplant.* 2007;22(12):3442–3450.
43. Otani H, et al. Antagonistic effects of bone morphogenetic protein-4 and -7 on renal mesangial cell proliferation induced by aldosterone through MAPK activation. *Am J Physiol Renal Physiol.* 2007;292(5):F1513–F1525.
44. Chan WL, Leung JC, Chan LY, Tam KY, Tang SC, Lai KN. BMP-7 protects mesangial cells from injury by polymeric IgA. *Kidney Int.* 2008;74(8):1026–1039.
45. Wang S, Hirschberg R. BMP7 antagonizes TGF-beta-dependent fibrogenesis in mesangial cells. *Am J Physiol Renal Physiol.* 2003;284(5):F1006–F1013.
46. Gould SE, Day M, Jones SS, Dorai H. BMP-7 regulates chemokine, cytokine, and hemodynamic gene expression in proximal tubule cells. *Kidney Int.* 2002;61(1):51–60.
47. Bell PD, Lapointe JY, Peti-Peterdi J. Macula densa cell signaling. *Annu Rev Physiol.* 2003;65:481–500.
48. Barajas L. Anatomy of the juxtaglomerular apparatus. *Am J Physiol.* 1979;237(5):F333–F343.
49. Lapointe JY, Laamarti A, Bell PD. Ionic transport in macula densa cells. *Kidney Int Suppl.* 1998; 67:S58–S64.
50. Navar LG, Inscho EW, Majid SA, Imig JD, Harrison-Bernard LM, Mitchell KD. Paracrine regulation of the renal microcirculation. *Physiol Rev.* 1996;76(2):425–536.
51. Navar LG, Ploth DW, Bell PD. Distal tubular feedback control of renal hemodynamics and autoregulation. *Annu Rev Physiol.* 1980;42:557–571.
52. Schnermann J, et al. Tubuloglomerular feedback: new concepts and developments. *Kidney Int Suppl.* 1998;67:S40–S45.
53. Tojo A, Onozato ML, Fujita T. Role of macula densa neuronal nitric oxide synthase in renal diseases. *Med Mol Morphol.* 2006;39(1):2–7.
54. Ren Y, Carretero OA, Garvin JL. Role of mesangial cells and gap junctions in tubuloglomerular feedback. *Kidney Int.* 2002;62(2):525–531.
55. Hugo C, Shankland SJ, Bowen-Pope DF, Couser WG, Johnson RJ. Extraglomerular origin of the mesangial cell after injury. A new role of the juxtaglomerular apparatus. *J Clin Invest.* 1997;100(4):786–794.
56. Gross O, et al. Preemptive ramipril therapy delays renal failure and reduces renal fibrosis in COL4A3-knockout mice with Alport syndrome. *Kidney Int.* 2003;63(2):438–446.
57. Koepke ML, Weber M, Schulze-Lohoff E, Beirowski B, Segerer S, Gross O. Nephroprotective effect of the HMG-CoA-reductase inhibitor cerivastatin in a mouse model of progressive renal fibrosis in Alport syndrome. *Nephrol Dial Transplant.* 2007;22(4):1062–1069.
58. Sugimoto H, Mundel TM, Sund M, Xie L, Cosgrove D, Kalluri R. Bone-marrow-derived stem cells repair basement membrane collagen defects and reverse genetic kidney disease. *Proc Natl Acad Sci U S A.* 2006;103(19):7321–7326.
59. Floege J, Kunter U, Weber M, Gross O. Bone marrow transplantation rescues Alport mice. *Nephrol Dial Transplant.* 2006;21(10):2721–2723.
60. Prodromidi EI, et al. Bone marrow-derived cells contribute to podocyte regeneration and amelioration of renal disease in a mouse model of Alport syndrome. *Stem Cells.* 2006;24(11):2448–2455.
61. Katayama K, et al. Irradiation prolongs survival of Alport mice. *J Am Soc Nephrol.* 2008;19(9):1692–1700.
62. Cosgrove D, et al. Collagen COL4A3 knockout: a mouse model for autosomal Alport syndrome. *Genes Dev.* 1996;10(23):2981–2992.
63. Yanagita M, et al. Gas6 regulates mesangial cell proliferation through Axl in experimental glomerulonephritis. *Am J Pathol.* 2001;158(4):1423–1432.
64. Kawachi H, Koike H, Kurihara H, Sakai T, Shimizu F. Cloning of rat homologue of podocin: expression in proteinuric states and in developing glomeruli. *J Am Soc Nephrol.* 2003;14(1):46–56.
65. Sado Y, et al. Establishment by the rat lymph node method of epitope-defined monoclonal antibodies recognizing the six different alpha chains of human type IV collagen. *Histochem Cell Biol.* 1995;104(4):267–275.
66. Valenzuela DM, et al. High-throughput engineering of the mouse genome coupled with high-resolution expression analysis. *Nat Biotechnol.* 2003;21(6):652–659.
67. Yanagita M, et al. Gas6 induces mesangial cell proliferation via latent transcription factor STAT3. *J Biol Chem.* 2001;276(45):42364–42369.
68. MacKay K, Striker LJ, Elliot S, Pinkert CA, Brinster RL, Striker GE. Glomerular epithelial, mesangial, and endothelial cell lines from transgenic mice. *Kidney Int.* 1988;33(3):677–684.
69. Rodgers KD, et al. Monocytes may promote myofibroblast accumulation and apoptosis in Alport renal fibrosis. *Kidney Int.* 2003;63(4):1338–1355.
70. Lories RJ, Derese I, Luyten FP. Modulation of bone morphogenetic protein signaling inhibits the onset and progression of ankylosing enthesitis. *J Clin Invest.* 2005;115(6):1571–1579.

LETTERS TO THE EDITOR

Successful treatment of membranoproliferative glomerulonephritis associated with hepatitis B and C virus simultaneous infection patient

A. Mima[1,2], N. Iehara[2], T. Matsubara[2], S. Yamamoto[2], H. Abe[1], K. Nagai[1], M. Matsuura[1], T. Murakami[1], S. Kishi[1], T. Araoka[1], F. Kishi[1], N. Kondo[1], R. Shigeta[1], K. Yoshikawa[1], T. Takahashi[1], T. Kita[3], T. Doi[1] and A. Fukatsu[2]

[1]Department of Nephrology, Institute of Health Biosciences, The University of Tokushima Graduate School, Tokushima, [2]Departments of Nephrology and [3]Cardiovascular Medicine, Kyoto University Graduate School of Medicine, Kyoto, Japan

Sir, – More and more epidemiological evidence suggests that hepatitis B virus (HBV) and hepatitis C virus (HCV) are associated with glomerular disease, the foremost being membranoproliferative glomerulonephritis (MPGN) [1].

Several histological findings have been reported in renal biopsies obtained from patients with glomerulonephritis including MPGN associated with chronic HBV infection, although the pathogenesis of hepatitis B glomerulonephritis remains unknown.

Administration of interferon-α and ribavirin are currently used in the treatment of MPGN associated with HCV [2], while only in few patients treatment of HBV related MPGN with interferon has been described. Moreover, there is even less evidence of treatment of MPGN associated with simultaneous HBV and HCV infection. Here, we report a case of proteinuria due to MPGN associated with simultaneous HBV and HCV infection.

A 62-year-old woman presented with edema of legs since 10 months and hypertension. Her significant medical history was a thoracoplasty due to tuberculosis with blood transfusion 44 years ago. At admission physical examination showed hypertension (160/90 mmHg). The liver and spleen were not palpable. She did not show any abnormalities in the neurologic tests. The laboratory findings were hemoglobin 10.4 g/dl, blood urea nitrogen (BUN) 23 mg/dl, creatinine 1.1 mg/dl with a creatinine clearance of 61 ml/min, total serum proteins 6.7 g/dl, albumin 3.9 g/dl, cholesterol 175 mg/dl, asparate aminotransferase 36 U/l, alanine aminotransferase 24 U/l, alkaline phosphatase 151 U/l, lactate dehydrogenase 266 U/l. Serological work-up showed C3 75.7 mg/dl, C4 8.9 mg/dl, and CH50 of < 7.0 U/ml. Immunoglobulins: IgG 1,592 mg/dl, IgA 151 mg/dl, IgM 139 mg/dl. Other serological data were normal or negative including CRP, ANA, double-strand DNA, ABGM, MPO- and PR3-ANCA. Cryoglobulinemia was found along with positive rheumatoid factor (35.6 IU/ml). Virologic studies were positive for HBs antigen and HBc and HBe antibody. HBV DNA and HCV RNA in serum were detected by quantitative polymerase chain reaction assay. The HBV DNA titer was 4.5 Log copy/ml. The HCV genotype was group Ib and HCV RNA titer showed 1,680 KU/ml. Urine examination revealed 3+ proteinuria and 24-h urinary protein was 2.2 g. On the fifth admission day, renal biopsy was performed. A specimen evaluated with light microscopy showed 2 of 14 glomeruli sclerosed. The glomeruli had diffuse hypercellularity with a marked increase in mesangial cells and matrix, resulting in an appearance of lobular formation. The glomerular capillary loops were thickened and double contours were recognized. There were no periodic acid-Schiff's (PAS)-positive deposits. Immunofluorescence analysis revealed granular capillary wall and mesangial regions staining that was predominantly for IgG with little IgM or C3. IgA and C1q were negative. These features were consistent with type I MPGN associated with HBV and HCV infection. A liver biopsy was not performed but there was no evidence of cirrhosis on ultrasound examination of the abdomen. Blood pressure control was poor despite treatment cilnidipine 20 mg once a day and amlodipine besilate 5 mg once a day. To reduce proteinuria and high blood pressure, olmesartan 40 mg once a day was initiated. In July 2006, therapy with interferon-α 40 μg per week and

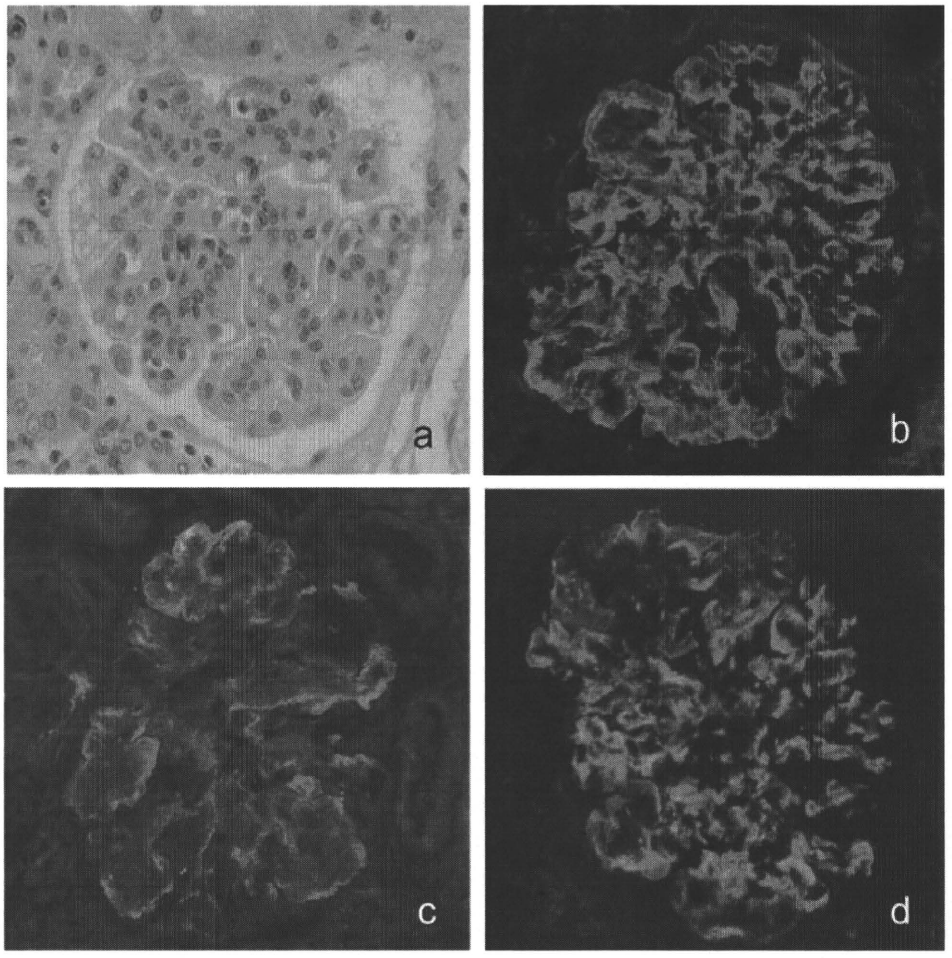

Figure 1. Light microscopic: Proliferation of endocapillary cells and mesangial cells as well as matrix are visible, resulting in a lobular formation appearance. (a) Periodic acid-Schiff stain. Original magnification × 400. Immunofluorescence microscopy, using polyclonal IgG antibodies, showing deposits only in the mesangium; these deposits were graded on a scale of 0 to 4+ as 3+ for IgG (b), 2+ for IgM (c), and 3+ for C3 (d). Original magnification × 400.

rivabirin 400 mg per day was started. After 6 weeks, despite the initially good clinical response, hemolytic anemia appeared and rivabirin was tapered off. 4 weeks later, anemia had improved and rivabirin was started again. We increased rivabirin to a dose of 800 mg/day 4 weeks after restarting rivabirin. In December 2006, the patient showed no appearance of HBV-DNA and HCV-RNA by quantitative blood analysis. One year after treatment, the patient was still in clinical and virologic remission.

This case suggests that the association of MPGN with chronic hepatitis is due to replicative HBV and HCV. The HCV associated CGN seems to be related to the glomerular deposition of immune complexes made by the HCV antigen, anti-HCV IgG antibodies, and a rheumatoid factor, which is an IgM kappa [3], while several studies reveal that patients with MPGN have a significant HBsAg carrier rate and report the pathogenesis to be immune complex mediated [4], though glomerular deposits of HBsAg may not be detectable as in our present case. The cause and effect relationship of HBV infection and glomerulonephritis could be proven only by demonstrating disappearance of the glomerular abnormalities on histology following seroconversion of virus after interferon therapy. In our case, HBV DNA had disappeared and clinical remission was prominent though seroconversion of HBV had not been achieved. Recently, it has been reported that interferon in HBV-associated glomerulonephritis achieved remission of proteinuria without seroconversion to anti-HBe [5]. The mechanism of remission of proteinuria using interferon in simultaneous

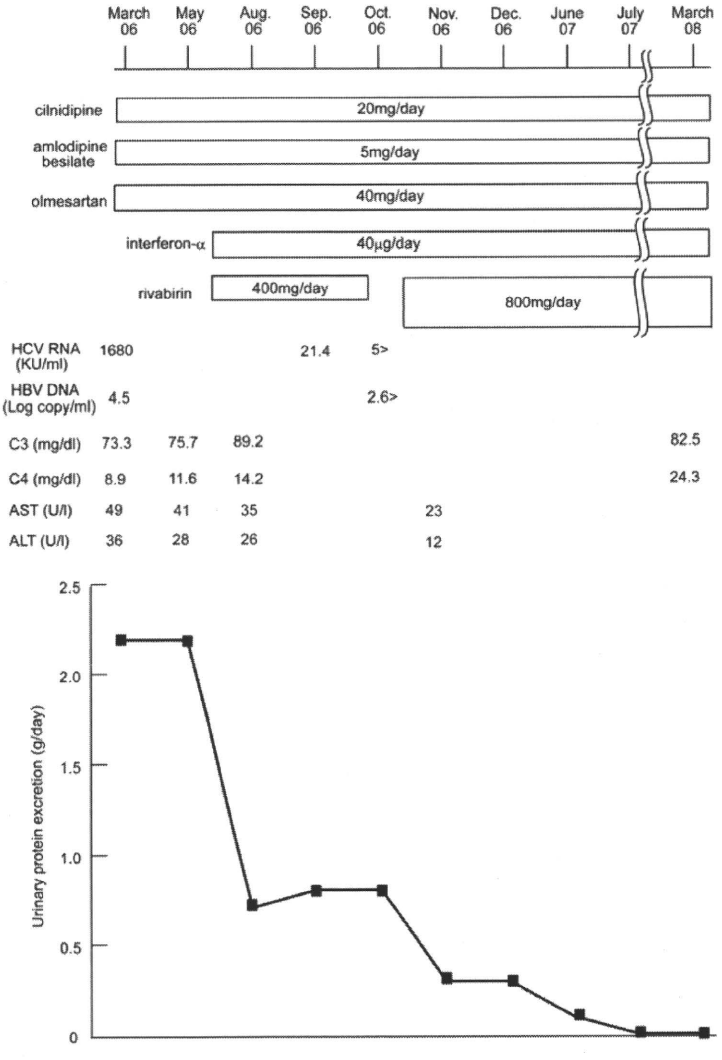

Figure 2. Clinical course of the patient.

HBV and HCV related glomerulonephritis is still unclear and requires further study.

Regarding treatment of HCV related glomerulonephritis, a combined therapy with interferon-α and ribavirin has become the standard treatment [6]. Once this combination therapy was started in our case, proteinuria and viremia were further decreased. Proteinuria dropped to a minimum level of 200mg per day 8 weeks after starting this therapy. HCV RNA titers were also significantly reduced. Owing to hemolytic anemia, ribavirin was stopped for a little while. Karmar et al. recommend to treat HCV related glomerulonephritis patients for at least 48 weeks and to continue the anti-viral therapy even in the absence of a decrease in HCV RNA concentration of 2 log at week 12 [7]. This is why we are now still continuing anti-viral therapy.

The present case demonstrated a patient with MPGN associated with simultaneous HBV and HCV infection. She achieved clinical remission under a full spectrum of drugs. We conclude that MPGN can be associated with simultaneous HBV and HCV infection and responds well to therapy with interferon-α and ribavirin.

References

[1] *Johnson RJ, Willson R, Yamabe H, Couser W, Alpers CE, Wener MH et al.* Renal manifestations of hepatitis C virus infection. Kidney Int. 1994; *46:* 1255-1263.

[2] *Johnson RJ, Gretch DR, Couser WG, Alpers CE, Wilson J, Chung M et al.* Hepatitis C virus-associated glomerulonephritis. Effect of alpha-interferon therapy. Kidney Int. 1994; *46:* 1700-1704.

[3] *Johnson RJ, Gretch DR, Yamabe H, Hart J, Bacchi CE, Hartwell P et al.* Membranoproliferative glomerulonephritis associated with hepatitis C virus infection. N Engl J Med. 1993; *328:* 465-470.

[4] *Johnson RJ, Couser WG.* Hepatitis B infection and renal disease: clinical, immunopathogenetic and therapeutic considerations. Kidney Int. 1990; *37:* 663-676.

[5] *Chung DR, Yang WS, Kim SB, Yu E, Chung YH, Lee Y et al.* Treatment of hepatitis B virus associated glomerulonephritis with recombinant human alpha interferon. Am J Nephrol. 1997; *17:* 112-117.

[6] *Alric L, Plaisier E, Thebault S, Peron JM, Rostaing L, Pourrat J et al.* Influence of antiviral therapy in hepatitis C virus-associated cryoglobulinemic MPGN. Am J Kidney Dis. 2004; *43:* 617-23.

[7] *Kamar N, Boulestin A, Selves J, Esposito L, Sandres-Saune K, Stebenet M et al.* Factors accelerating liver fibrosis progression in renal transplant patients receiving ribavirin monotherapy for chronic hepatitis C. J Med Virol. 2005; *76:* 61-68.

A. Mima, MD, PhD
Department of Nephrology
Institute of Health Biosciences
The University of Tokushima Graduate School
Tokushima 770-8503, Japan
akiramima@clin.med.tokushima-u.ac.jp

HUMAN MUTATION Mutation in Brief 32: E1976-E1984 (2010) Online

MUTATION IN BRIEF

HUMAN MUTATION

OFFICIAL JOURNAL
HGVS
HUMAN GENOME VARIATION SOCIETY
www.hgvs.org

Maternal Riboflavin Deficiency, Resulting in Transient Neonatal-Onset Glutaric Aciduria Type 2, Is Caused by a Microdeletion in the Riboflavin Transporter Gene *GPR172B*

Gladys Ho[1,3], Atsushi Yonezawa[4], Satohiro Masuda[4], Ken-ichi Inui[4], Keow G. Sim[2], Kevin Carpenter[2,3], Rikke K.J. Olsen[5], John J. Mitchell[6], William J. Rhead[7], Gregory Peters[2,3], and John Christodoulou[1,2,3,*]

[1] Genetic Metabolic Disorders Research Unit; [2] Western Sydney Genetics Program, Children's Hospital at Westmead 2145, Sydney, Australia; [3] Discipline of Paediatrics & Child Health, University of Sydney, Sydney 2006, Australia; [4] Dept of Pharmacy, Kyoto University Hospital, Kyoto, Japan; [5] Research Unit for Molecular Medicine, Aarhus University Hospital and Faculty of Health Sciences, Skejby Sygehus, Aarhus, Denmark; [6] Dept of Genetics, Montreal Children's Hospital, Montreal, Canada; [7] Medical Genetics Center, Children's Hospital of Wisconsin, Milwaukee, WI, USA

*Correspondence to Professor John Christodoulou, Western Sydney Genetics Program, Children's Hospital at Westmead, Locked Bag 4001, Westmead, NSW, 2145, Australia. Phone: +61 2 9845 3452, Fax: + 61 2 9845 1864, E-mail: johnc@chw.edu.au

Communicated by Elizabeth Neufeld

ABSTRACT: Riboflavin, or vitamin B2, is a precursor to flavin adenine dinucleotide (FAD) and flavin mononucleotide (FMN) molecules, required in biological oxidation-reduction reactions. We previously reported a case of a newborn female who had clinical and biochemical features of multiple acyl-CoA dehydrogenation deficiency (MADD), which was corrected by riboflavin supplementation. The mother was then found to be persistently riboflavin deficient, suggesting that a possible genetic defect in riboflavin transport in the mother was the cause of the transient MADD seen in the infant. Two recently-identified riboflavin transporters G protein-coupled receptor 172B (*GPR172B* or *RFT1*) and riboflavin transporter 2 (*C20orf54* or *RFT2*) were screened for mutations. Two missense sequence variations, c.209A>G [p.Q70R] and c.886G>A [p.V296M] were found in *GPR172B*. *In vitro* functional studies of both missense variations showed that riboflavin transport was unaffected by these variations. Quantitative real-time PCR revealed a *de novo* deletion in *GPR172B* spanning exons 2 and 3 in one allele from the mother. We postulate that haploinsufficiency of this riboflavin transporter causes mild riboflavin deficiency, and when coupled with nutritional riboflavin deficiency in pregnancy, resulted in the transient riboflavin-responsive disease seen in her newborn infant. This is the first report of a genetic defect in riboflavin transport in humans. ©2010 Wiley-Liss, Inc.

KEY WORDS: RFT1, RFT2, GPR172B, riboflavin transport, MADD

Received 19 August 2010; accepted revised manuscript 19 October 2010.

DOI: 10.1002/humu.21399

INTRODUCTION

Riboflavin or vitamin B2 is a water-soluble vitamin essential for normal cellular functions. It is a precursor in the synthesis of flavin mononucleotide (FMN) and flavin adenine dinucleotide (FAD), both of which are important molecules in biological reduction-oxidation reactions (Powers, 2003). In particular, FAD is a cofactor for the electron transfer flavoprotein (ETF) and ETF ubiquinone oxidoreductase (ETF:QO) making up the electron transport pathway for a number of mitochondrial flavoprotein dehydrogenases (most of which are acyl-CoA dehydrogenases) mainly involved in fatty acid and amino acid metabolism. A defect in either ETF or ETF:QO causes multiple acyl-CoA dehydrogenation deficiency (MADD), or glutaric aciduria type 2 (MIM# 231680). This is an autosomal recessive disorder with mutations commonly found in the two genes encoding the two subunits of ETF (*ETFA*; MIM# 608053, and *ETFB*; MIM# 130410), or in *ETFDH* (MIM# 231675) which encodes ETF:QO (Indo et al., 1991; Beard et al., 1993; Colombo et al., 1994; Goodman et al., 2002). The clinical phenotype varies from severe neonatal onset with congenital anomalies and early death to mild and/or later onset forms (Rhead et al., 1987). Some patients respond dramatically to pharmacological doses of riboflavin, in particularly those with mutations in the *ETFDH* gene (Olsen et al., 2007; Law et al., 2009).

We now report on a novel genetic mutation in the mother of a neonatal case of suspected MADD, the latter of whom had no identifiable genetic defects in *ETFA*, *ETFB* or *EFTDH*. A newborn female presented on the first day of life with clinical and biochemical findings consistent with MADD. Riboflavin supplementation corrected the biochemical abnormalities 24 hours after commencing the vitamin. The mother was subsequently shown to be persistently riboflavin-deficient. We postulated that a primary genetic defect in one of the recently identified riboflavin transporter genes in the mother was the cause of the transient MADD in the infant, and that such defect would be absent in the infant.

MATERIALS AND METHODS

The clinical details of this family have been previously reported (Chiong et al., 2007). In brief, a female infant (III:1 – Figure 1), the first child of nonconsanguineous parents of Australian and Maltese background, presented within the first 24 hr of life with clinical features and urinary organic acids highly suggestive of multiple acyl-CoA dehydrogenase deficiency (MADD). Urine metabolic screening performed on day 2 showed a typical dicarboxylic aciduria with gross increases in hexandioate, octandioate, decanediaoate and decenedioate, moderate increases in ethylmalonate, glutarate, 2-hydroxyglutarate, 5-hydroxyhexandioate and 7-hydroxyoctanedioate. Hexanoylglycine was also markedly increased but no other acylglycines were detected. Blood spot screening from the baby on day 2 by tandem mass spectrometry showed normal acylcarnitines, C4-carnitine, 0.52 and 0.45 μmol/L (cut off 1.3 μmol/L), C10-carnitine, 0.76 μmol/L and 0.63 μmol/L (cut off 1 μmol/L), C10:1-carnitine, 0.39 μmol/L and 0.21 μmol/L (cut off 1 μmol/L), C14-carnitine, 0.73 μmol/L and 0.7 μmol/L (cut off 1 μmol/L), C14:1-carnitine, 0.6 and 0.51 (cut off 1), C16-carnitine, 1.91 μmol/L and 1.93 μmol/L (cut off 11 μmol/L), C6-carnitine 0.37 μmol/L and 0.27 μmol/L (cut off 1 μmol/L) and C5D-carnitine 0.21 μmol/L and 0.22 μmol/L (cut off 0.3 μmol/L). C12 – carnitine was not measured in the blood spots. Plasma carnitine and acylcarntine levels on day 2 were: total – 26 mmol/L (normal range [NR] 8 – 45), free – 11 (NR 4 – 33), glutarylcarnitine – 0.40 (NR 0 – 0.16), hexanoylcarnitine – 0.2 (NR 0 – 0.1), octanoylcarnitine – 0.4 (NR 0 – 0.4), decaonylcarnitine – 0.9 (NR 0 – 0.4), decenoylcarnitine – 0.2 (0 – 0.2), dodecanoylcarnitine – 1.15 (NR 0 – 0.34), tetradecenoylcarnitine – 1.08 (NR 0 – 0.27), tetradecanoylcarnitine – 0.77 (NR 0 – 0.19), palmitoylcarnitine – 0.91 (NR 0 – 0.74).

Remarkably, within 24 hr of the commencement of resuscitative therapy, including oral riboflavin, her clinical condition improved dramatically and her chemistry returned to normal. Fibroblast ETF and ETF:QO enzymology of cells cultured in riboflavin replete or depleted medium were all normal, making MADD highly unlikely. Riboflavin was ceased at 15 months of age, and now aged 5 yrs she has remained healthy with no further episodes of metabolic decompensation and with normal urinary organic acids and plasma acylcarnitines.

Based on these findings, her mother (II:1 – Figure 1) was suspected of having riboflavin deficiency, and this was confirmed biochemically. Initially, the low riboflavin level was thought to be nutritional in origin, but sustained correction of the plasma acylcarnitines in the mother only when she continued oral riboflavin therapy led to the conclusion that she was likely to have a primary genetic defect of riboflavin transport or metabolism. Her husband (II:2) and parents (I:1 and I:2) had normal riboflavin levels, urinary organic acids and plasma acylcarnitines. A second child (III:2) had normal urine organic acids, plasma acylcarnitines and riboflavin levels at 1 month of age. During the pregnancy with this child the mother (II:1) had been on riboflavin supplementation.

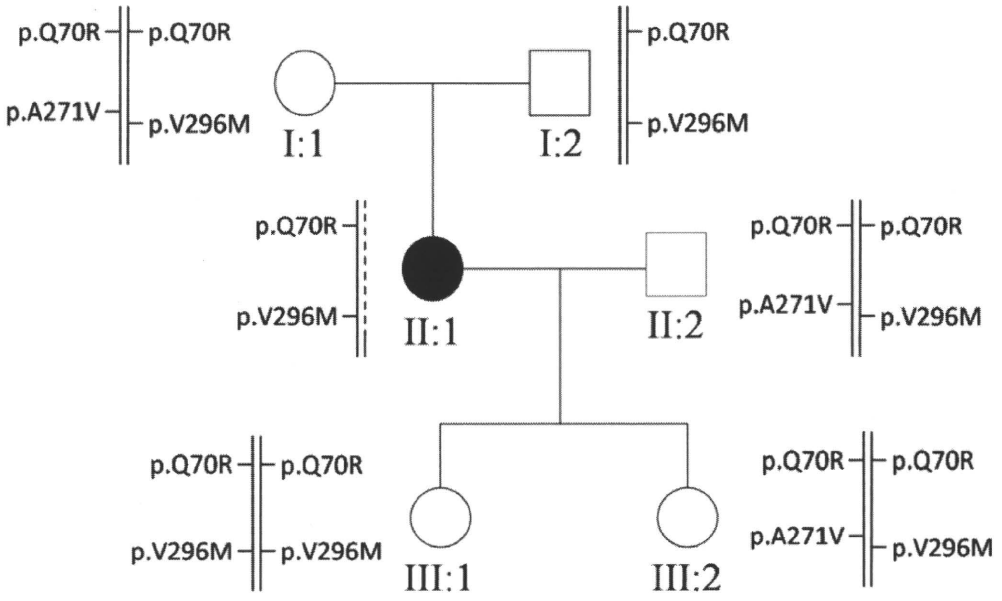

Figure 1. Pedigree and Haplotypes of Family with Riboflavin Deficiency. Pedigree of the family, showing I:1, maternal grandmother, I:2, maternal grandfather, II:1, riboflavin-deficient mother (in black), II:2, father; III:1, infant with transient riboflavin deficiency; III:2, unaffected infant. I:1, I:2, II:2 and III:2 had normal plasma acylcarnitines and riboflavin levels. Schematic diagrams of the *GPR172B* gene show the haplotypes of each family member for the three polymorphisms, p.Q70R, p.A271V and p.V296M. The dashed line represents the position of the region deleted in the pathogenic allele in II:1.

We postulated that a primary genetic defect in riboflavin metabolism or transport in the mother was the cause of the transient MADD in the infant III:1, and that such defect would be absent in the infant. Mutations in *ETFA*, *ETFB* and *ETFDH* have been previously excluded (Chiong et al., 2007). We also excluded mutations of FAD synthesis in the riboflavin kinase (*RFK*) and FAD synthetase (*FLAD1*) genes as the cause of riboflavin deficiency. The newly identified human riboflavin transporters, G protein-coupled receptor 172B (*GPR172B;* MIM# 607883) or riboflavin transporter 1 (*RFT1*) (Yonezawa et al., 2008) and riboflavin transporter 2 (*C20orf54* or *RFT2*; MIM# 613350) (Yamamoto et al., 2009) were screened for mutations that may potentially lead to riboflavin deficiency. *GPR172B*, a 2.8 kb gene located at chr17p13.2, contains 5 exons and has two mRNA transcript variants (GenBank reference numbers NM_001104577.1 and NM_071986.3). The two transcripts differ only in the 5' untranslated region (5' UTR) and encode the same protein of 448 amino acids (NP_001098047.1 and NP_060456.3). Nucleotide numbering reflects cDNA numbering with +1 corresponding to the A of the ATG translation initiation codon in the reference sequences, according to journal guidelines (www.hgvs.org/mutnomen). The initiation codon is codon 1.

These studies were approved by the Ethics Committee of the Children's Hospital at Westmead, and informed consent was obtained from the parents of the proband. Using the genomic DNA of the riboflavin-deficient mother (II:1), the four coding exons (exons 2 - 5) in *GPR172B* were screened using direct sequencing (Macrogen, Seoul, Korea). Primers and PCR conditions are available upon request. Two single nucleotide polymorphisms were identified in exon 3 of *GPR172B*.

In order to exclude pathogenicity of the two mutations, the *in vitro* function of the two mutated GPR172B proteins was characterized. Experimental procedures were previously described (Yonezawa et al., 2008). Briefly, human *GPR172B* cDNA was subcloned into pcDNA3.1/Hygro(+) plasmid vector. Site-directed mutations in *GPR172B* gene was introduced with QuikChange II Site-Directed Mutagenesis Kit (Agilent Technologies, Santa Clara, CA) and the mutations were confirmed by direct sequencing. HEK 293 cells were seeded onto poly-D-lysine-coated 24-well plates at a density of 7.5 x 10^4 cells per well. The cells were transfected with 200 ng of plasmid DNA per well using 1 μl of LipofectAMINE 2000 (Life Technologies, Carlsbad, CA). Forty-eight hours after the transfection, the cells were used for the subsequent experiments. Cells were incubated in the incubation buffer containing 10 nM [^{3}H]riboflavin (0.903 TBq/mmol, Moravek Biochemicals, Inc., Brea, CA) for 1 min, and then washed twice with ice cold incubation buffer. The cells were solubilized in 0.5 N NaOH, and the radioactivity was measured by liquid scintillation counting. The composition of the incubation buffer was as follows: 145 mM NaCl, 3 mM KCl, 1 mM $CaCl_2$, 0.5 mM $MgCl_2$, 5 mM D-glucose and 5 mM HEPES (adjusted with NaOH to pH 7.4).

In order to identify any copy number variations in *GPR172B*, primers were designed using Primer3 software (Rozen and Skaletsky, 2000) at five different sites along the length of *GPR172B*, with two pairs of primers spanning the locations of the missense mutations in exon 3, and one pair of primers in the remaining coding exons (exons 2, 4 and 5), as well as a pair of primers in a remote genomic region as a reference. Primer sequences are available upon request. Real-time PCR was performed using a Rotorgene 6000 (Corbett Life Sciences, now QIAGEN, Doncaster, Vic, Australia). Each reaction of 10 μl contained 0.5 U Hotmaster Taq polymerase (5 PRIME, Hamburg, Germany), 1x Hotmaster Taq buffer provided with polymerase, 0.2 mM of each dNTP (Invitrogen, Carlsbad, CA), 0.5 μM of each primer, 0.5 M betaine (Sigma-Aldrich, Castle Hill, NSW, Australia), 5.0% DMSO (Sigma-Aldrich, Castle Hill, NSW, Australia), 1x SYBR green dye (Invitrogen, Carlsbad, CA) and 25 ng genomic DNA. The PCR program conditions were as follows: initial denaturation at 94°C for 4 min, followed by 40 cycles of 94°C for 20s, 56°C for 20s and 70°C for 30s, with a fluorescence measurement at the end of each 70°C elongation step. Analysis of qPCR was carried out as previously described (Pfaffl, 2001).

RESULTS

Two previously reported single nucleotide polymorphisms (SNP) in exon 3 of *GPR172B* were identified (GenBank reference NC_000017.9), both of which were apparently homozygous in II:2, as shown in Figure 2. The first was a transition from an adenine residue to guanine at cDNA position 209 resulting in a missense mutation at glutamine 70 to arginine (c.209A>G; p.Q70R). The second was a transition from a guanine to adenine at c.886, changing valine 296 to methionine (c.886G>A; p.V296M). Both missense mutations have previously been reported in the dbSNP (reference ID for c.209A>G rs346822, c.886G>A rs2304445).

The uptake of riboflavin of three mutant GPR172B proteins was investigated along with the wild-type protein: p.Q70R, p.V296M and a third containing both p.Q70R and p.V296M. Results are shown in Figure 3. There were no significant differences between the rates of uptake of any of the three mutant proteins compared to the wild-type GPR172B.

A further possibility is the occurrence of a large deletion that would not be detectable by PCR and direct sequencing. We used a quantitative PCR (qPCR) strategy to search for heterozygous deletions in *GPR172B*, which revealed a partial deletion of the *GPR172B* gene in the riboflavin-deficient mother II:1. Figure 4 shows reduced copy numbers of exon 2 and both regions tested in exon 3, indicating that II:1 carries one intact and one truncated copy of GPR172B, whereas the infant III:1 has two intact copies. Array CGH using the Human Genome CGH Microarray 244A (Agilent Technologies, Inc. Santa Clara CA) array did not detect any deletions in II:1 (data not shown), limiting the size of the deletion to a maximum of 1.9 kb. We were unable to define the exact position of the breakpoints of the deletion.

Additional screening of other family members at these loci revealed that infant III:1 was homozygous for p.Q70R and for p.V296M. Infant III:2 and the father (II:2) of the infants III:1 and III:2 and infant III:2 were homozygous for p.Q70R and heterozygous for p.V296M. The genotype and quantitative PCR results for the infant III:1 is consistent with our hypothesis that she has not inherited the deleterious allele from II:1. The maternal grandfather I:2 was heterozygous for p.Q70R and for p.V296M. The maternal grandmother I:1 was homozygous for p.Q70R and heterozygous for p.V296M. It was not possible to determine from which parental chromosome the partial deletion of *GPR172B* in II:1 has arisen. Screening also revealed a third common SNP at c.812C>T (p.A271V, rs346821), heterozygous in the father, the infant III:2 and the maternal grandmother. Genotype data are

summarized in Figure 1. Biochemical testing for the father, infant III:2 and maternal grandparents revealed normal plasma acylcarnitines and riboflavin levels.

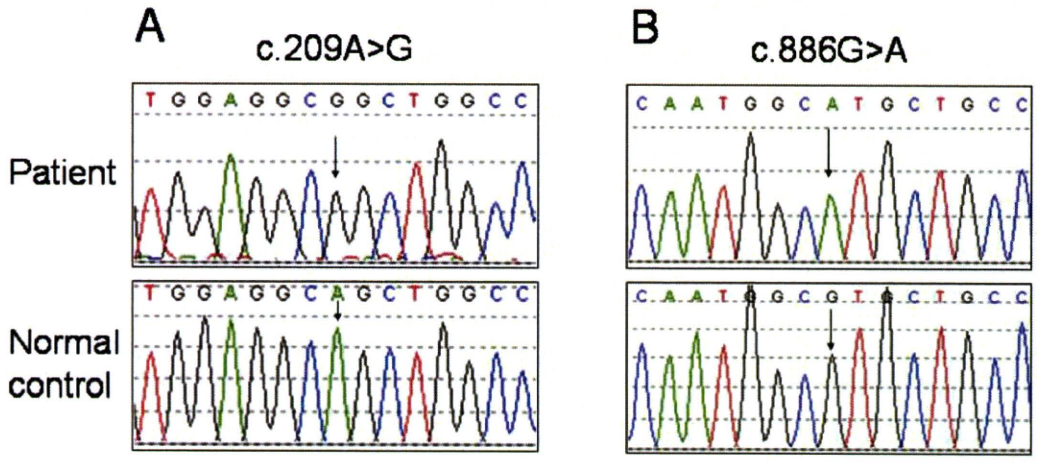

Figure 2. *GPR172B* Missense Mutations c.209A>G (p.Q70R) and c.886G>A (p.V296M). (A) Chromatograms showing the apparently homozygous change in the riboflavin-deficient mother II:1 from the genomic reference sequence (adenine, top panel) to guanine (bottom panel) at cDNA position c.209. (B) Chromatograms showing the apparently homozygous change in the riboflavin-deficient mother II:1 from the genomic reference sequence (guanine, top panel) to adenine (bottom panel) at cDNA position c.886.

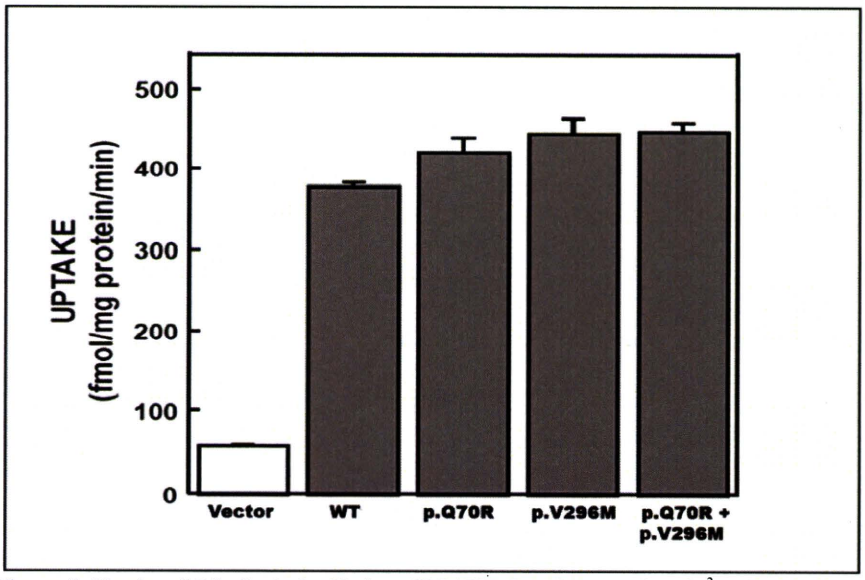

Figure 3. Uptake of Riboflavin by Variant GPR172B Proteins. Uptake of [^{3}H]riboflavin (10 nM) in HEK293 cells transfected with pcDNA3.1/Hygro(+) plasmids containing wild-type (WT) or variant (p.Q70R alone, p.V296M alone, or combined p.Q70R and p.V296M) *GPR172B* cDNA. No significant differences were found between the wild-type protein and any of the variant proteins. Data are presented as mean +/- SE (n=3).

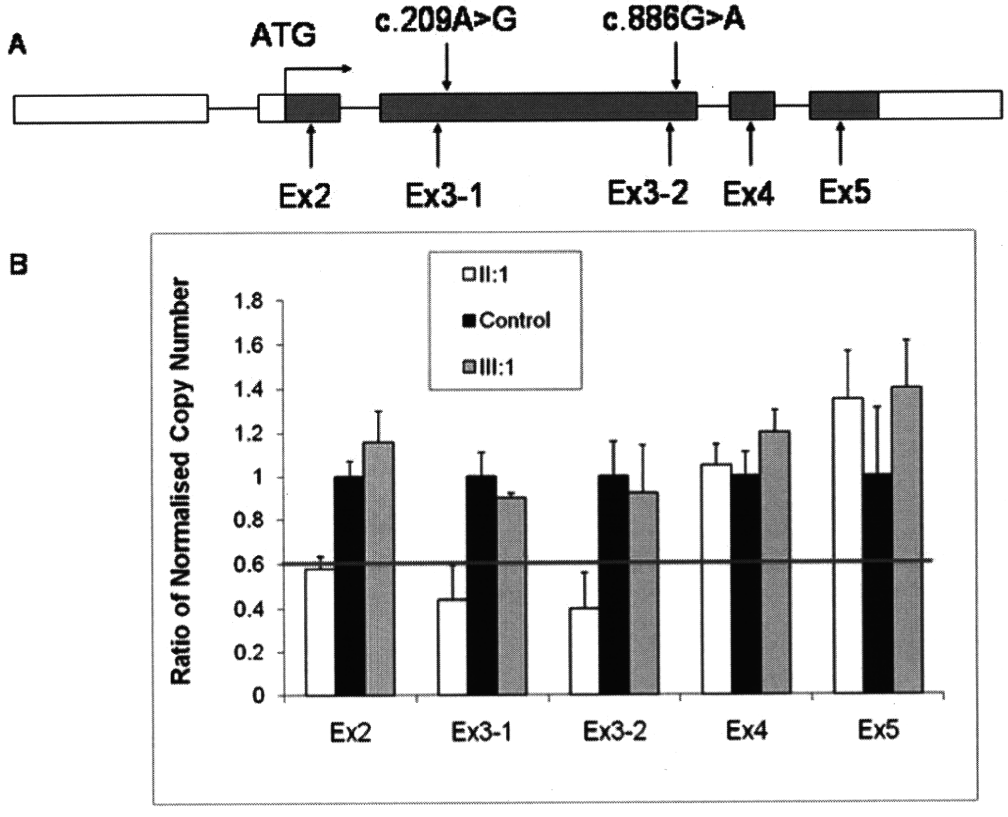

Figure 4. Structure of *GPR172B* and Relative Copy Number in II:1 and III:1. (A) Schematic diagram of the arrangement of exons in *GPR172B* on chromosome 17, showing the five exons (box), with the coding regions highlighted in grey and the untranslated regions in white. Introns are indicated by a line. The initiation ATG codon is marked as shown. The two missense sequence variations detected in the riboflavin-deficient mother (II:1) are indicated by arrows above the gene. The arrows below the gene mark the locations of the primers used for the quantitative PCR studies to identify copy number variations. (B) Normalised copy numbers for five regions of *GPR172B* in riboflavin-deficient mother (white bars) and infant (grey) relative to 3 controls from normal population (black). The threshold for a deletion is 0.6 (solid line). The riboflavin-deficient mother carried a deletion over the regions of Ex2, Ex3-1 and Ex3-2, whilst Ex4 and Ex5 showed normal copy numbers. The infant did not carry any deletions in this locus. Data are presented as means +/- SD (n = 4).

DISCUSSION

We hypothesized that a genetic defect in the riboflavin-deficient mother II:1 was responsible for the transient MADD-like phenotype observed in the infant III:1. Screening of the recently discovered riboflavin transporter *GPR172B* revealed a heterozygous deletion of exons 2 and 3. This deletion was identified only in the mother, but not the infant, in accordance with our hypothesis. The deletion is also *de novo*, inferred from the presence of heterozygous SNPs in both parents of II:1 at the same location. The initiation codon of *GPR172B* is located in exon 2, and therefore the deletion of exons 2 and 3 is likely to completely disrupt expression of GPR172B from that allele. We surmise that the haploinsufficiency is the cause of the mild riboflavin deficiency observed in II:1.

We also identified two missense mutations which are unlikely to have any pathogenic effects on riboflavin transport. The observed rates of riboflavin uptake of different alleles of GPR172B, expressed *in vitro*, suggest that neither the two missense mutations individually, p.Q70R or p.V296M, nor the combination of both p.Q70R and

p.V296M in *cis*, has any effect on the functionality of the GPR172B protein (Figure 3). In addition, *in silico* splicing prediction suggested that neither variation would affect exon splicing.

The frequencies of these alleles in normal populations lend further support to their non-pathogenicity. The genotypic frequency of homozygous p.Q70R is 94.5%, suggesting that the p.R70 is the predominant allele. Alignment of GPR172B to its homologues reveals that p.R70 is the ancestral allele (data not shown). Although the genotypic frequency of homozygous p.V296M is lower (only 1.8%), it is more common than the prevalence of MADD. The screening of the other family members (summarized in Figure 1) and biochemical testing also suggest that the missense mutations p.Q70R and p.V296M are not the genetic causes for riboflavin deficiency.

The second riboflavin transporter gene *C20orf54* (*RFT2*) was also screened, with eleven variations identified (Table 1). We excluded pathogenicity in the only nonsynonymous change identified (data not shown). Large genomic deletions were excluded by the presence of heterozygous variations throughout the length of the gene.

Table 1. Variations in *RFT2* identified in individual II:1

Systematic name [a]	Predicted protein effect [b]	Status [c]	Location	dbSNP entry [d]
c.-14_-6del9	p.M1?	Heterozygous	5' UTR	rs11467076
c.321C>T	p.=	Heterozygous	Exon 2	rs3746808
c.456C>T	p.=	Heterozygous	Exon 2	rs3746807
c.765C>T	p.=	Heterozygous	Exon 3	rs3746805
c.800C>T	p.P267L	Heterozygous	Exon 3	rs3746804
c.1073+21A>T	no change to splicing	Heterozygous	Intron 3	n/a
c.1197+106A>G	no change to splicing	Homozygous	Intron 4	rs6054589
c.1197+108C>T	no change to splicing	Heterozygous	Intron 4	rs3746801
c.1233T>C	p.=	Homozygous	Exon 5	rs910857
c.*16delC		Heterozygous	3' UTR	rs3215628

[a] Systematic name designations based on GenBank reference sequence NM_033409.3. Nucleotide numbering reflects cDNA numbering with +1 corresponding to the A of the ATG translation initiation codon in the reference sequences, according to journal guidelines (www.hgvs.org/mutnomen).

[b] Protein changes based on GenPept reference sequence NP_212134.3, with initiation codon numbered 1; splicing predictions by Berkeley Drosophila Genome Project Splice Site Predictor, http://www.fruitfly.org/seq_tools/splice.html

[c] Status in individual II:1

[d] dbSNP, http://www.ncbi.hlm.nih.gov/projects/SNP/

In contrast to previous disorders involving riboflavin metabolism, the case we have reported is a dominant disorder with a very mild phenotype. None of the usual symptoms of riboflavin deficiency were observed in the mother II-2, and the deficiency was only detected biochemically. This may be in part due to a compensatory effect of at least one other riboflavin transporter, RFT2 (Yamamoto et al., 2009). *RFT2* is expressed predominantly in the small intestine, and is thought to be the primary transporter involved in riboflavin uptake (Yamamoto et al., 2009). The manifestation of the MADD-like phenotypes in only the infant can be attributed to the greater demand for nutrients in the growing fetus, as well as the high expression level of *GPR172B* in placenta (Yonezawa et al., 2008), suggesting that its main role may be placental transport of riboflavin.

To our knowledge, this is the first description of a genetic defect involving riboflavin uptake in humans. Although there are no similar parallels in human, the mouse ascorbic acid (vitamin C) transporter Slc23a1 shows a similar gene dosage response, with heterozygote mice having a reduced level of ascorbic acid compared to wild-type, and with homozygous wildtype offspring of heterozygous females showing mild ascorbic acid deficiency (Sotiriou et al., 2002). Interestingly, supplementation of ascorbic acid of heterozygous females during pregnancy normalizes ascorbic acid levels in the newborn pups, except for those homozygous for the mutation (Sotiriou et al., 2002).

It is interesting to note that the second child, III:2, had no postnatal problems and testing confirmed her to be riboflavin replete. Her mother continued riboflavin supplementation throughout the pregnancy. We conclude that the maternal riboflavin supplementation protected the second infant from the consequences of riboflavin deficiency.

In conclusion, a deletion spanning exons 2 and 3 of the riboflavin transporter *GPR172B* was identified in the mother of the infant initially suspected of MADD. The deletion was not present in the infant, indicating that transient clinical and metabolic abnormalities in the infant were a consequence of maternal riboflavin deficiency. Genes involved in cellular riboflavin metabolism/transport have previously been suggested to be associated with riboflavin-responsive forms of MADD (Rhead et al., 1993; Vergani et al., 1999), but identification of mutations have until now been limited to *EFTA*, *EFTB* and *EFTDH*. For patients with MADD and without mutations in these three genes, screening of *GPR172B*, and indeed the second riboflavin transporter *RFT2*, should be considered.

ACKNOWLEDGMENTS

We would like to thank the family described in this report who very kindly allowed us to obtain samples for testing on a number of occasions. This study was supported in part by a grant-in-aid for Scientific Research (KAKENHI) from the Ministry of Education, Science, Culture and Sports of Japan.

WEB RESOURCES

Berkeley Drosophila Genome Project Splice Site Predictor, http://www.fruitfly.org/seq_tools/splice.html
dbSNP, http://www.ncbi.hlm.nih.gov/projects/SNP/
GenBank, http://www.ncbi.hlm.nih.gov/Genbank/
Online Mendelian Inheritance in Man (OMIM), http://www.ncbi.nlm.nih.gov/Omim/

REFERENCES

Beard SE, Spector EB, Seltzer WK, Frerman FE, Goodman SI. 1993. Mutations in electron transfer flavoprotein:ubiquinone oxidoreductase (ETF:QO) in glutaric acidemia type II (GA2). Clin Res 41: 271A.

Chiong MA, Sim KG, Carpenter K, Rhead WJ, Ho G, Olsen RKJ, Christodoulou J. 2007. Transcient multiple acyl-CoA dehydrogenation deficiency in a newborn female cause by maternal riboflavin deficiency. Mol Genet Metab 92: 109-114.

Colombo I, Finocchiaro G, Garavaglia B, Garbuglio N, Yamaguchi S, Frerman FE, Berra B, DiDonato S. 1994. Mutations and polymorphisms of the gene encoding the â-subunit of the elctron transfer flavoprotein in three patients with glutaric acidemia type II. Hum Mol Genet 3: 429-435.

Goodman SI, Binard RJ, Woontner MR, Frerman FE. 2002. Glutaric acidemia type II: gene structure and mutations of the electron transfer flavoprotein:ubiquinone oxidoreductase (ETF:QO) gene. Mol Genet Metab 77: 86-90.

Indo Y, Glassberg R, Yokota I, Tanaka K. 1991. Molecular characterization of variant alpha subunit of electron transfer flavoprotein in three patients with glutaric acidemia type II and identification of glycine substitution for valine-157 in the sequence of the precursor, producing an unstable mature protein in a patient. Am J Hum Genet 49: 575-580.

Law L-K, Tang NLS, Hui J, Fung SLM, Ruiter J, Wanders RJA, Fok T-F, Lam CWK. 2009. Novel mutations in *ETFDH* gene in Chinese patients with riboflavin-responsive multiple acyl-CoA dehydrogenase deficiency. Clin Chim Acta 404: 95-99.

Olsen RKJ, Olpin SE, Andresen BS, Miedzybrodzka ZH, Pourfarzam M, Merinero B, Frerman FE, Beresford MW, Dean JCS, Cornelius N, Andersen O, Oldfors A, Holme E, Gregersen N, Turnbull DM, Morris AAM. 2007. *ETFDH* mutations as a major cause of riboflavin-responsive multiple acyl-CoA dehydrogenation deficiency. Brain 130: 2045-2054.

Pfaffl MW. 2001. A new mathematical model for relative quantification in real-time RT-PCR. Nucleic Acids Res 29: e45.

Powers HJ. 2003. Riboflavin (vitamin B-2) and health. Am J Clin Nutr 77: 1352-1360.

Rhead WJ, Roettger V, Marshali T, Amendt B. 1993. Multiple acyl-coenzyme A dehydrogenation disorder responsive to riboflavin: substrate oxidation, flavin metabolism, and flavoenzyme acvitivites in fibroblasts. Pediatr Res 33: 129-135.

Rhead WJ, Wolff JA, Lipson M, Falace P, Desai N, Fritchman K, Moon A, Sweetman L. 1987. Clinical and biochemical variation and family studies in the multiple acyl-CoA dehydrogenation disorders. Pediatr Res 21: 371-376.

Rozen S, Skaletsky HJ. 2000. Primer3 on the WWW for general users and biological programmers. In: Krawetz S, Misener S, editors. Bioinformatics Methods and Protocols: Methods in Molecular Biology. Totowa, NJ: Humana Press p 365-386.

Sotiriou S, Gispert S, Cheng J, Wang Y, Chen A, Hoogstraten-Miller S, Miller GF, Kwon O, Levine M, Guttentag SH, Nussbaum RL. 2002. Ascorbic-acid transporter Slc23a1 is essential for vitamin C transport into the brain and for perinatal survival. Nature Medine 8: 514-517.

Vergani L, Barile M, Angelini C, Burlina AB, Nijtmans L, Freda MP, Brizio C, Zerbetto E, Dabbeni-Sala F. 1999. Riboflavin therapy: Biochemical heterogeneity in two adult lipid storage myopathies. Brain 122: 2401-2411.

Yamamoto S, Inoue K, Ohta K-y, Fukatsu R, Maeda J-y, Yoshida Y, Yuasa H. 2009. Identification and functional characterization of rat riboflavin transporter 2. J Biochem 145: 437-443.

Yonezawa A, Masuda S, Katsura T, Inui K-i. 2008. Identification and functional characterization of a novel human and rat riboflavin transporter, RFT1. Am J Physiol Cell Physiol 295: C632-C641.

OPEN ACCESS Freely available online

PLoS one

Activation of Src Mediates PDGF-Induced Smad1 Phosphorylation and Contributes to the Progression of Glomerulosclerosis in Glomerulonephritis

Akira Mima[1,3], Hideharu Abe[1]*, Kojiro Nagai[1], Hidenori Arai[2], Takeshi Matsubara[3], Makoto Araki[3], Kazuo Torikoshi[3], Tatsuya Tominaga[1], Noriyuki Iehara[3], Atsushi Fukatsu[3], Toru Kita[4], Toshio Doi[1]

1 Department of Nephrology, Institute of Health Biosciences, University of Tokushima Graduate School, Tokushima, Japan, **2** Department of Geriatric Medicine, Kyoto University Graduate School of Medicine, Kyoto, Japan, **3** Department of Nephrology, Kyoto University Graduate School of Medicine, Kyoto, Japan, **4** Department of Cardiovascular Medicine, Kyoto University Graduate School of Medicine, Kyoto, Japan

Abstract

Platelet-derived growth factor (PDGF) plays critical roles in mesangial cell (MC) proliferation in mesangial proliferative glomerulonephritis. We showed previously that Smad1 contributes to PDGF-dependent proliferation of MCs, but the mechanism by which Smad1 is activated by PDGF is not precisely known. Here we examined the role of c-Src tyrosine kinase in the proliferative change of MCs. Experimental mesangial proliferative glomerulonephritis (Thy1 GN) was induced by a single intravenous injection of anti-rat Thy-1.1 monoclonal antibody. In Thy1 GN, MC proliferation and type IV collagen (Col4) expression peaked on day 6. Immunohistochemical staining for the expression of phospho-Src (pSrc), phospho-Smad1 (pSmad1), Col4, and smooth muscle α-actin (SMA) revealed that the activation of c-Src and Smad1 signals in glomeruli peaked on day 6, consistent with the peak of mesangial proliferation. When treated with PP2, a Src inhibitor, both mesangial proliferation and sclerosis were significantly reduced. PP2 administration also significantly reduced pSmad1, Col4, and SMA expression. PDGF induced Col4 synthesis in association with increased expression of pSrc and pSmad1 in cultured MCs. In addition, PP2 reduced Col4 synthesis along with decreased pSrc and pSmad1 protein expression in vitro. Moreover, the addition of siRNA against c-Src significantly reduced the phosphorylation of Smad1 and the overproduction of Col4. These results provide new evidence that the activation of Src/Smad1 signaling pathway plays a key role in the development of glomerulosclerosis in experimental glomerulonephritis.

Citation: Mima A, Abe H, Nagai K, Arai H, Matsubara T, et al. (2011) Activation of Src Mediates PDGF-Induced Smad1 Phosphorylation and Contributes to the Progression of Glomerulosclerosis in Glomerulonephritis. PLoS ONE 6(3): e17929. doi:10.1371/journal.pone.0017929

Editor: Sudha Agarwal, Ohio State University, United States of America

Received November 17, 2010; **Accepted** February 20, 2011; **Published** March 22, 2011

Funding: This research is supported by Grants-in-Aid for Scientific Research of the Japan Society for the Promotion of Science (no. 21591033 and 19590973). The funders had no role in study design, data collection and analysis, decision to publish, or preparation of the manuscript.

Competing Interests: The authors have declared that no competing interests exist.

* E-mail: abeabe@clin.med.tokushima-u.ac.jp

Introduction

Glomerulonephritis is usually progressive and remains an important cause of end stage renal disease. In sclerosing glomerulonephritis, accumulation of the extracellular matrix (ECM) is a critical process in progressive glomerular injuries [1,2]. Type IV collagen (Col4) is one of the most important components of the expanded ECM [3]. Moreover, smooth muscle α actin (SMA) is a known common molecular marker of phenotypic changes of mesangial cells (MCs) in many glomerular diseases. We previously reported that Smad1 participates in the development of glomerulosclerosis in experimental glomerulonephritis [4]. We also reported that Smad1 transcriptionally regulates the expression of Col4 and SMA [5,6]. However, the mechanisms by which Smad1 is activated in glomerulonephritis have not been fully elucidated.

Platelet-derived growth factor (PDGF) is known to be a critical mitogen for MCs in vitro and in vivo [1,7]. It is noteworthy that mice deficient for PDGF B or PDGF receptor show abnormal glomeruli due to a lack of MC development [8–11]. Several lines of evidence indicate that PDGF plays a key role in the development of glomerulosclerosis not only in experimental models but also in human glomerular diseases [12,13]. The introduction of a neutralizing anti-PDGF antibody has shown that both mesangial proliferation and glomerulosclerosis can be markedly ameliorated in a rat glomerulonephritis model [14]. Moreover, we previously showed that the development of glomerulosclerosis from mesangial proliferation is dependent on PDGF-induced Smad1 activation [4], but little is known concerning the regulatory mechanisms of Smad1 activation by PDGF in glomerulonephritis. c-Src is a ubiquitously expressed non-receptor protein-tyrosine kinase [15] that is involved in multiple pathways regulating cell growth, migration, and survival [16]. c-Src is also an important component of the PDGF signal transduction pathway [17]. Several reports have demonstrated that PDGF plays a key role in MC proliferation and glomerulopathy *in vivo* and *in vitro* [7,18,19]. Previously we demonstrated that Smad1 is phosphorylated by PDGF in MCs [4]. However, the exact role of c-Src in MCs as well as in glomerulonephritis remains unclear.

In the present study, we demonstrated that c-Src is activated in experimental proliferative glomerulonephritis and that the reduction of c-Src ameliorates the development of glomerulosclerosis by blocking of the Smad1 signal transduction pathway. We further

showed that c-Src plays an important role as a switch molecule for the activation of Smad1 downstream of PDGF signaling. These findings unveil the molecular mechanisms underlying the induction of MC proliferation and MC phenotype alteration, resulting in proliferative glomerulonephritis. Taking these results together, we hypothesized that the Src/Smad1 pathway may be critical in the pathogenesis of proliferative glomerulonephritis.

Materials and Methods

Animals

Full details of the animal experimental protocols were approved and ethical permission was granted by the Review Board of Kyoto University (Permit Number: Med Kyo 08508). We used age-matched male Wistar rats (8 to 12 weeks old, 180 to 200 g) bred at the Shimizu Laboratory Animal Center (Hamamatsu, Japan). The animals were housed under specific pathogen-free conditions at the Animal Facility of Kyoto University. Levels of serum creatinine and blood urea nitrogen were measured using a Hitachi Mode 736 autoanalyzer. The urinary albumin concentrations were measured from 24-h urine collections by Nephrat and Albuwell (Exocell), according to the manufacturer's protocols.

Cell culture experiments

A glomerular mesangial cell line was established from glomeruli isolated from normal 4-week-old mice (C57BL/6JxSJL/J) and was identified according to a method described previously [7]. The MCs were plated on 100-mm plastic dishes (Nunc) that were maintained in B medium (a 3:1 mixture of minimal essential medium/F12 modified with trace elements) supplemented with 1 mM glutamine, penicillin at 100 units/ml, streptomycin at 100 μg/ml, and 10% fetal calf serum (Irvine Scientific). The cells were passaged weekly with trypsin-EDTA. The cultured cells fulfilled the previously described criteria generally accepted for glomerular mesangial cells [20]. Stimulation with angiotensin II (Ang II) (Sigma), PDGF, PP2 (Calbiochem, Darmstadt, Germany), or olmesartan (Cosmo Bio, Tokyo, Japan) was carried out in DMEM containing 0.5% FCS at 37°C for the indicated times. A rat monoclonal anti-PDGFβ-receptor antibody (APB5) and its antagonistic effects on the PDGFβ-R signal transduction pathway in vitro have been described previously [4].

Constructs, transfection, and co-immunoprecipitation

Src cDNAs (pUSE Src wild type, pUSE Src kinase mutant, and empty vector) were obtained from Upstate Biotechnology, Inc. (Lake Placid, NY). MCs were transfected using FuGene6 (Roche, Mannheim, Germany) according to the manufacturer's protocol. After 48 h of transfection, the cells were washed with PBS, and 1 ml ice-cold lysis buffer (25 mM Tris-HCl pH 7.4, 100 mM NaCl, 2 mM EDTA, 0.5% Nonidet P-40, Complete protease inhibitors cocktail; Roche) was added. For co-immunoprecipitation assay, whole cell lysates were first pre-cleared with protein G–Sepharose (Amersham) and followed by incubation with anti-PDGFR antibody (Santa Cruz) for 3 h at 4°C. The immune complex was isolated and separated by SDS–PAGE and analyzed by Western bot analysis. Protein was detected using polyclonal rabbit anti-Src antibody (Cell Signaling Technology).

Histology and Immunohistochemistry

Tissues were fixed in Methyl Carnoy's solution and were paraffin-embedded. Multiple sections were prepared and stained with periodic acid silver methenamine (PASM) and periodic acid-Schiff's reagent (PAS). Immunohistochemical staining was performed with antibodies specific to Col4 (Progen) or SMA (Abcam), using an established avidin-biotin detection method (Vector Laboratories). Frozen sections were used for the detection of pSrc and pSmad1 (Cell Signaling Technology). Glomerular morphometry was evaluated in PASM-stained tissues. The glomerular surface area and the PASM-positive area/glomerular area (%) were measured using an image analyzer with a microscope (IPAP, Sumitomo Chemical, Osaka, Japan) as previously described [21–24]. To quantitatively measure the expression of pSrc and pSmad1, pSrc-positive or pSmad1-positive cells/DAPI-positive nuclei were counted, and the mean percentages of pSrc-positive or pSmad1-positive cells were calculated. An investigator scored sections in a blinded fashion, according to an established scoring system (range 0–4; 0, no ECM deposition; 4, ECM deposition in all sections of the glomeruli) to semiquantify the localization of Col4 and SMA.

Small-interfering RNA

MCs (0.5×10^5) were seeded into 12-well plates (Nunc) and were grown until they were 60% to 80% confluent. The small-interfering RNAs (siRNAs) for c-Src, Smad1, and LRP1 (Dharmacon) or control scrambled siRNA (Dharmacon) were combined with DharmaFECT transfection reagent (Dharmacon), and the cells were transfected according to the recommended protocol with siRNA (100 nM final concentration). After 48 h of transfection, cells were starved in DMEM containing 0.5% BSA before treatment. After 48 h of incubation, the cells were stimulated with or without PDGF (Calbiochem).

TGFβ-neutralizing antibody assay

MCs were resuspended at a concentration of 1×10^6 cells/ml and plated onto 100-mm dish either in the presence of 10 μg/ml TGFβ-neutralizing antibody (R&D Systems) or a control normal chicken IgY. After 24 h of incubation, the cells were treated with PDGF for additional 12 h and were harvested and underwent protein extraction on Western blotting.

Western blotting

Isolated glomerular MCs were suspended in RIPA buffer (50 mM Tris, pH 7.5, 150 mM NaCl, 1% Nonidet P-40, 0.25% SDS, 1 mM Na_3VO_4, 2 mM EDTA, 1 mM phenylmethylsulfonyl fluoride, 10 mg/ml of aprotinin) and incubated for 1 h at 4°C. After centrifugation, the supernatants were used as total cell lysates. Twenty micrograms of each sample was applied to SDS-PAGE. After electrophoresis, the proteins were transferred to nitrocellulose filters (Schleicher & Schuell). The blots were subsequently incubated with anti-phospho-Smad1, anti-phspho-Src (Cell Signaling Technology), anti-SMA, anti-LRP1 (Abcam) or anti-Col4 antibody (Progen), followed by incubation with horseradish peroxidase-conjugated goat anti-rabbit IgG and sheep anti-mouse IgG (Amersham). The immunoreactive bands were visualized using horseradish peroxidase-conjugated secondary antibody and the enhanced chemiluminescent system (Amersham). These bands were quantified using an imaging densitometer (Science Lab 99 Image Gauge, Fujifilm, Tokyo, Japan).

Data analysis

The data are expressed as the mean ± S.D. Comparison among more than two groups was performed by one-way analysis of variance (ANOVA), followed by post hoc analysis (Bonferroni/Dunn test) to evaluate the statistical significance between the two groups. All analyses were performed using StatView (SAS Institute, Cary, NC). Statistical significance was defined as $P<0.05$.

Results

Glomerular phosphorylation of c-Src and Smad1 parallels the progress of glomerulosclerosis in rat Thy1 GN

We utilized a model of mesangial proliferative glomerulonephritis, known as anti-Thy1-induced glomerulonephritis (Thy1 GN), which exhibits sclerosis in the glomeruli. The renal function of Thy1 GN on day 6 was significantly decreased (Figure S1A). MC proliferation began on day 3 and glomerulosclerosis began on day 6. Renal damage clearly regressed until day 15. Sclerosis in the kidney peaked on day 6 and sclerotic changes subsided until day 15 (Figure 1A and B). Localization of phospho-Src (pSrc) and phospho-

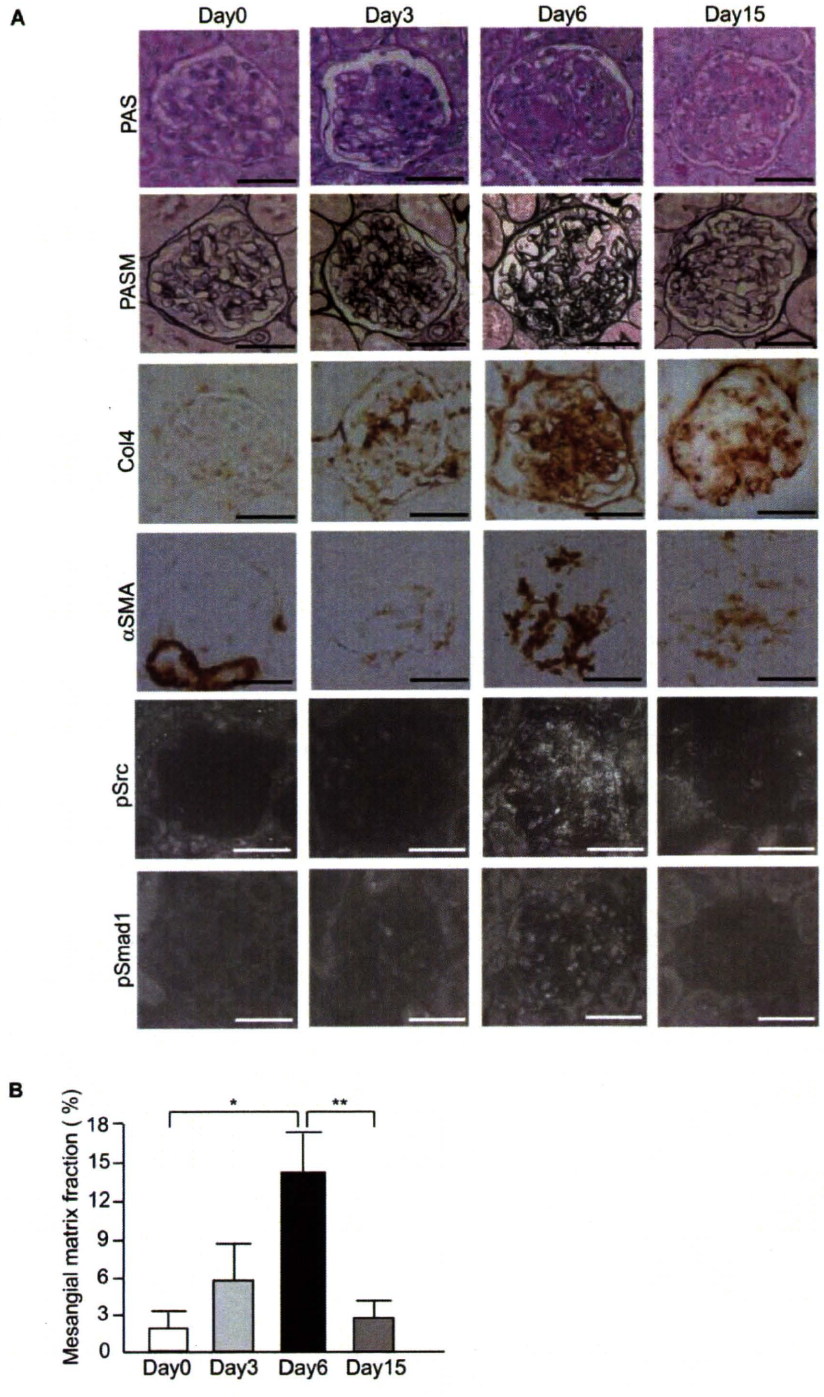

Figure 1. Induction and activation of c-Src and Smad1 in proliferative glomerulonephritis. (A) Representative light-microscopic appearance and immunohistochemistry of glomeruli in Thy1 GN. Scale bars = 100 μm. (B) Quantitative assessment of PASM staining in Thy1 GN. *$P = 0.002$, **$P = 0.002$).
doi:10.1371/journal.pone.0017929.g001

Smad1 (pSmad1) in the nuclei was scant on day 0. On day 3, phosphorylation began in c-Src and Smad1 proteins. The level of phosphorylation gradually increased and positively stained nuclei in parallel with the activity of mesangial proliferation during the development of glomerulosclerosis. Phosphorylation peaked on day 6 and then decreased towards day 15 (Figure 2, C, D and E). Phosphorylation of c-Src and Smad1 was almost undetectable on day 0 but became prominent during the proliferative stages in Thy1 GN, peaked on day 6, and then decreased towards day 15 (Figure 2C, D and E). In addition, the expression of Col4 and SMA changed in parallel with the activation of c-Src and Smad1 (Figure 2A, B and E). These data suggest that both Smad1 and c-Src are activated in the course of proliferative injuries in rat kidneys.

PP2 preserves renal function and attenuates glomerulosclerosis in rat glomerulonephritis

To investigate whether the c-Src/Smad1 pathway plays a pivotal role in developing glomerulosclerosis, we administered a Src specific inhibitor, PP2, to Thy1 GN rats from days 0 to 6 and assessed glomerulosclerosis on day 6. Untreated Thy1 GN rats showed an increased degree of glomerulosclerosis, whereas glomerulosclerosis was significantly decreased in the PP2-treated group (Figure 3A, B), along with renal function (Figure 3, C–E).

PP2 represses the activation of Smad1 and the expression of both Col4 and SMA in rat glomerulonephritis

Next, to examine the effect of PP2 on the morphological changes seen in Thy1 GN glomerulosclerosis, we examined Col4 and SMA expression in the two groups. PP2 treatment significantly inhibited Col4 and SMA expression, whereas expression was increased in the non-treatment group (Figure 3F). Moreover, we examined whether PP2 affected the phosphorylation and translocation of c-Src and Smad1 in Thy1 GN rats. PP2 treatment inhibited the phosphorylation of c-Src and Smad1, and their expression was localized in the nucleus in untreated Thy1 GN (Figure 3F). These data from immunohistochemistry were confirmed by Western blot analysis (Figure 3G).

Effect of PP2 on PDGF-mediated signaling in MCs

Because PDGF is well known to play a key role in the development of glomerulosclerosis, we investigated whether PDGF can activate c-Src/Smad1 signal transduction and increase the synthesis of Col4. Expression of Col4, pSrc, and pSmad1 was induced by PDGF stimulation in MCs cultured for 12 hours (Figure 4A–D). These inductions were inhibited by PP2 treatment

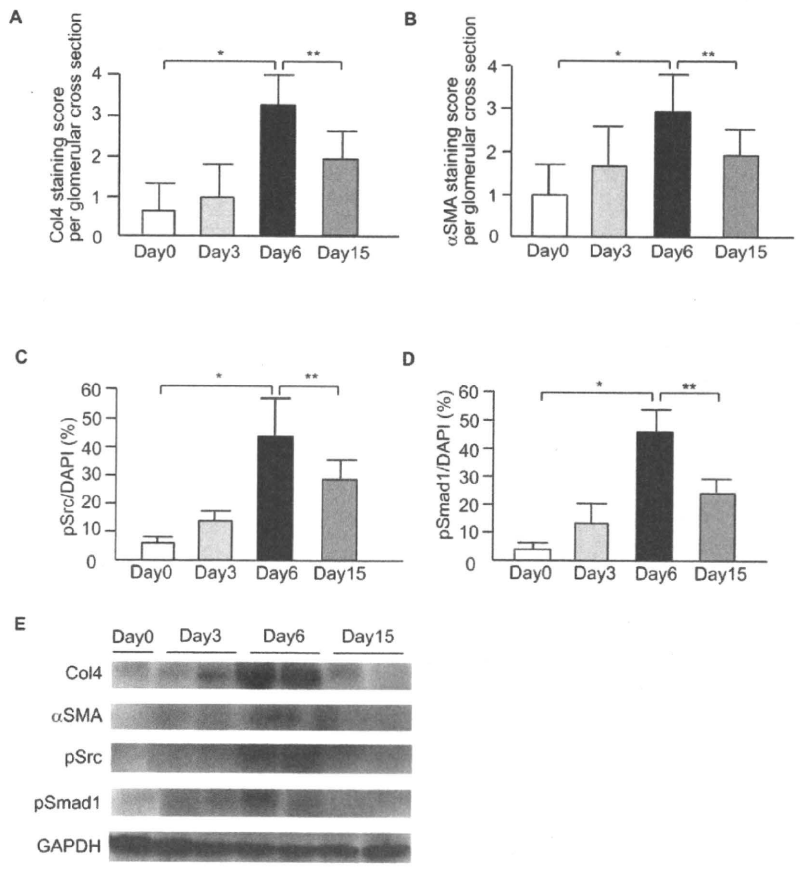

Figure 2. Time course of glomerular expression of Col4, SMA, pSrc and pSmad1 in Thy1 GN. (A, B) Staining scores per glomerular cross-section for Col4 (*$P<0.001$, **$P<0.001$) and SMA (*$P<0.001$ and **$P=0.009$) were calculated. Data represent mean values ± S.D. of at least three independent experiments; n = 6 for each experimental group. (C, D) Quantification of glomerular pSrc and pSmad1 by optical densitometry. The pSrc-positive nuclei and pSmad1-positive nuclei were counted in 10 consecutive fields in each specimen and normalized by the number of DAPI-positive nuclei. *$P<0.001$, **$P<0.001$. (E) Western blot for the glomerular lysates from each group. Data represent mean values ± S.D. of at least three independent experiments; n = 6 for each experimental group.
doi:10.1371/journal.pone.0017929.g002

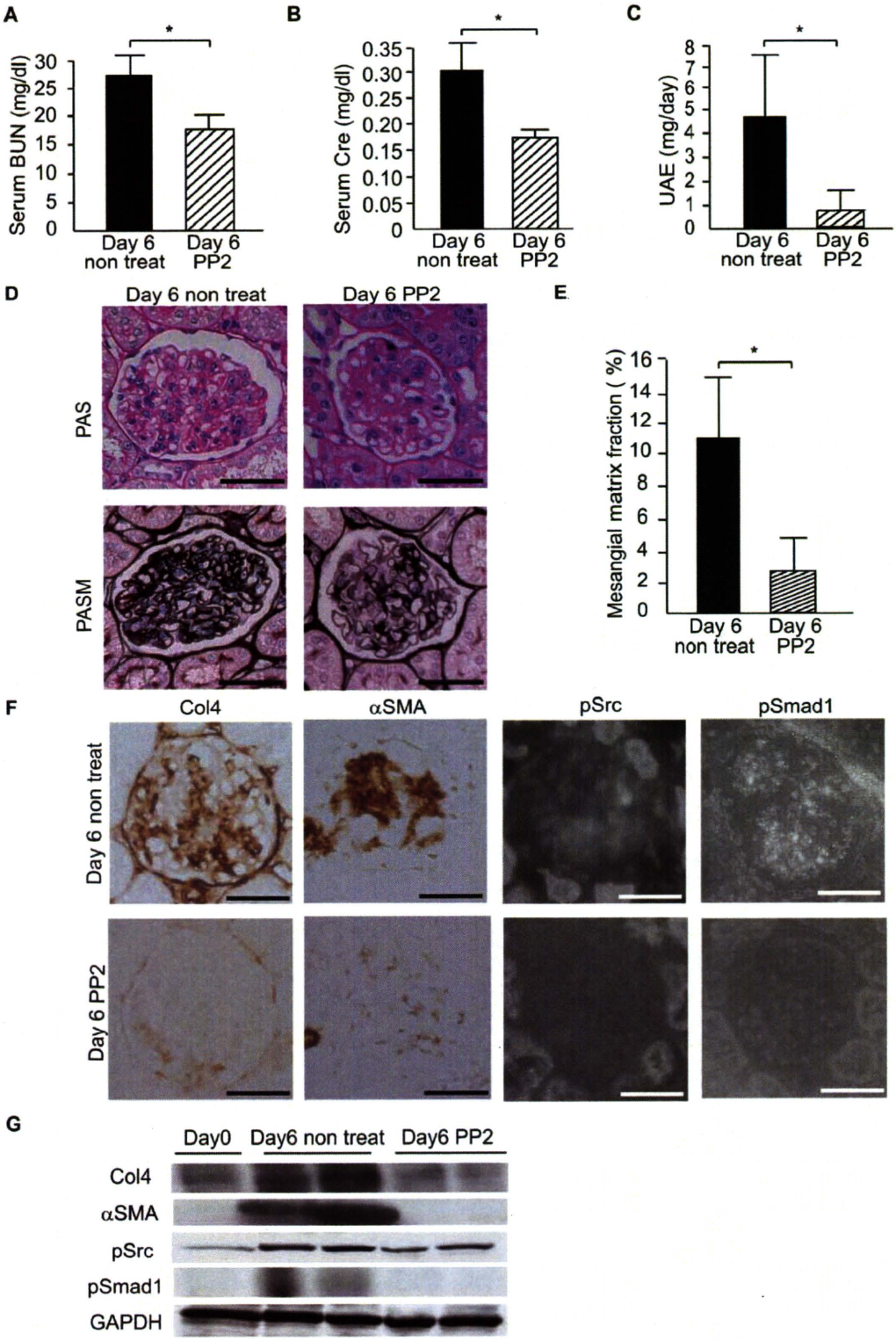

Figure 3. Src-specific inhibitor PP2 inhibits glomerulosclerosis and glomerular expression of pSrc and pSmad1 in Thy1 GN. (A–C) Serum blood urine nitrogen (BUN), serum creatinine (Cre), and UAE in the nontreatment and PP2 groups. *P* values were 0.001, 0.001 and 0.017, respectively. (D, E) Representative light-microscopic appearance of glomeruli (PAS and PASM staining) and quantitative assessment of PASM staining in Thy1 GN with or without PP2 on day 6. Scale bars = 100 μm. *$P<0.001$. (F) Immunohistochemistry of glomeruli (Col4, SMA, pSrc and pSmad1) in Thy1 GN with or without PP2 on day 6. Scale bars = 100 μm; n = 6 for each experimental group. (G) Western blot for the glomerular lysates from each group. Data represent mean values ± S.D. of at least three independent experiments; n = 6 for each experimental group on day 6.
doi:10.1371/journal.pone.0017929.g003